Nonpoint Source Nutrient Pollution Study in Baffin Bay Texas, Phase I

Final Report

GLO Contract No. 20-036-000-B744
September 10, 2021

Prepared by:

Dorina Murgulet, Principal Investigator
J. David Felix, Co-Principal Investigator
Cody V. Lopez, Laboratory Technician
Yixi Qui, Graduate Research Assistant

With support from:

Chrissy Barrera, Graduate Research Assistant
Christopher Vickers, Graduate Research Assistant
Anthony Cox, Graduate Research Assistant
William Wolfe, Graduate Research Assistant
Bimal Gyawali, Graduate Research Assistant
Valeriu Murgulet, Co-Investigator

Texas A&M University-Corpus Christi
6300 Ocean Dr., Unit 5850
Corpus Christi, Texas 78412
Phone: 361-825-2309
Email: Dorina.murgulet@tamucc.edu

Submitted to:
Texas General Land Office
1700 Congress Ave.
Austin, TX 78701-1495

A report funded by a Texas Coastal Management Program Grant approved by the Texas Land Commissioner pursuant to National Oceanic and Atmospheric Administration Award No. NA19NOS4190106

CONTENTS

ABBREVIATIONS

ft	feet
cm	centimeter
m	meter
km	kilometer
hr	hour
d	day
s	second
$cm \cdot d^{-1}$	centimeter per day
$m \cdot s^{-1}$	meters per second
$m^3 \cdot s^{-1}$	cubic meters per second
$km^3 \cdot d^{-1}$	cubic kilometers per day
$mg \cdot L^{-1}$	milligrams per liter
$\mu g \cdot L^{-1}$	microgram per liter
µL	microliters
mL	milliliter
µM	micro Molar
$mol \cdot L^{-1}$	mole per liter
$\mu mol \cdot L^{-1}$	micromoles per liter
$\mu mol \cdot d^{-1}$	micromoles per day
DO	dissolved oxygen
SGD	submarine groundwater discharge
^{222}Rn	radon-222
^{223}Ra	radium-223
^{224}Ra	radium-224
^{226}Ra	radium-226
$Bq \cdot m^{-3}$	Becquerels per cubic meter
ERT	electrical resistivity
CRP	continuous resistivity profile
Ω-m	ohm-meter
TA	total alkalinity
DIC	dissolved inorganic carbon
DOC	dissolved organic carbon
N	nitrogen
TDN	total dissolved nitrogen
DIN	dissolved inorganic nitrogen
DON	dissolved organic nitrogen
NO_3^-	nitrate
NO_2^-	nitrite
NOx	nitrate + nitrite
NH_4^+	ammonium
HPO_4^{2-}	phosphate
$HSiO_3$	silica
chl-α	chlorophyll-α

FIGURE LEGEND

TABLE LEGEND

Table 1: $\delta^{15}N$ values of reported DON sources and local DON sources. Local livestock waste is $\delta^{15}N$-TDN (Campbell, 2018; Choi et al., 2017; Cornell et al., 1995; Curt et al., 2004; Lee et al., 2012; Russell et al., 1998). *Local value from Campbell 2018 and local septic included from this study's well samples.

EXECUTIVE SUMMARY

Results of this study indicate that sewage or septic effluent is the dominant DON source to the nearshore Laguna Salada in Baffin Bay, regardless of the proximity to septic system/residential area (Riviera Fishing Peer -RP) or underdeveloped, more agricultural dominated area (Laguna Salada Research Site 55-S site). The high sewage/septic influence can be attributed to septic effluent release to groundwater and/or wastewater discharge to surface water, but high DON concentrations and enriched δ^{15}N-DON in the groundwater strongly support the former. The sewage/septic contribution at RP (46.4 ± 4.7%) and LS 46.5 ± 7.2%) do not show significant differences. Overall, the highest sewage/septic contributions were observed in summer (June, July, and August) and fall (September, October, and November). The high pulse of submarine groundwater discharge (SGD)-related DON (and NH_4^+) in summer to early fall could be attributed to these observed inputs.

Both surface water locations at LS exhibit the least sewage/septic contribution (37.5 ± 0.1%) but highest fertilizer (18.2 ± 0%), livestock waste (21.7 ± 0.1%) and atmospheric deposition (22.7 ± 0.2%) contribution in spring (March, April, and May). This is potentially the result of higher precipitation (the highest amounts for the duration of the study occurred in May), which is followed by an increase in SGD rates, only slightly shy to the rates following Hurricane Hanna. The least sewage/septic contribution (42.5 ± 3.0%) but highest fertilizer (16.9 ± 0.6%), livestock waste (20.0 ± 1.1%) and atmospheric deposition (20.7 ± 1.5%) contribution at RP was estimated in winter (December, January, and February). This can be explained by SGD-derived inputs that seemed to be elevated by Hurricane Hanna at the end of July and the additional precipitation in September. In winter, when precipitation is much lower, and riverine/surface runoff input is also lower, DON SGD fluxes were among the lowest measured, also reflected by

the lower surface water concentrations. In this season, the relative contribution of fertilizer, livestock waste and atmospheric deposition to the surface water DON pool were the highest. A decreased flux of nearshore SGD leads lo lower inputs of septic and in turn decreases the SGD-derived DON flux but increase the contribution of fertilizer, livestock waste and atmospheric deposition. This is expected to bring in more inputs of NOx and NH_4^+, as indicated by the SGD-derived fluxes of these solutes, which as opposed to DON, are increasing in fall and winter.

BACKGROUND AND RELEVANCE

Ancillary Information

The Laguna Madre Estuary, a unique ecosystem that sustains a ~ $225 million tourism and fishing industry (Coastal Bay Bends and Estuary Program, 2015), has been affected by declining water quality and harmful algal blooms (HABs) in recent years. The brown tide, first recorded here in 1989 (Buskey et al., 2001), is unique to more traditionally studied HABs (e.g., red tide) in that the organisms can flourish on dissolved organic nitrogen (DON) as a nutrient source, which allows the tide to persist where other organism populations would fail. Recent efforts by the Baffin Bay Volunteer Water Quality Monitoring Study have recorded average DON levels in the bay to be ~10X that of dissolved inorganic nitrogen (DIN); ideal nutrient conditions for the brown tide to flourish. These previous efforts have provided information on conditions leading to HABs and insight to areas in the bay where nutrients are concentrating, but they did not provide direct evidence of nutrient sources.

A 2016 CMP study, by Dr. Murgulet's group at Texas A&M University-Corpus Christi (TAMU-CC), indicates that bay-wide submarine groundwater discharge (SGD) contributed, in $\mu mol \cdot d^{-1}$, up to $3.3x10^{14}$ (mainly in the form of ammonium [NH_4^+]) in July and $0.5x10^{14}$ in November of DIN, $1.2x10^{14}$ in July and $0.7x10^{14}$ in November of DOC, and $0.4x10^{14}$ DON in November (DON data were not available for July), which are 3 to 5 orders of magnitude greater than surface runoff (Murgulet, 2018). For comparison, the typical concentrations of NO_x ($NO_2^- + NO_3^-$) in Baffin Bay range from <0.3 µM to 35 µM with an average concentration of <1-4 µM, and NH_4^+ concentrations ranged from 7 µM to 91.7 µM in surface water over the years 2013-2015 (Wetz, 2015). According to Wetz (2015), surface water DON regularly exceeded 35 µM. Since it is clear from the previous efforts that nutrient inputs are orders of magnitude higher in

the bay bottom sediments than any surface fluxes, this study focused on determining and quantifying the sources and processing of nutrients along transport paths to the bay, accomplished by analysis of stable nitrogen isotopic composition in combination with groundwater transport and residence times. The distinct isotopic ratios of nitrogen (nitrate: NO_3^-, NH_4^+, DON) sources were used to fingerprint and quantify nutrient sources (i.e., nutrients entering groundwater from atmospheric deposition or fertilizer, sewage, etc.) and processing mechanisms (i.e., remineralization) in estuaries, bays, oceans, and rivers (Hadas et al., 2009; Knapp et al., 2011b; Schlarbaum et al., 2010).

Furthermore, to develop an accurate conceptual model of nutrient inputs to the bay, the groundwater inputs were measured at two locations in Laguna Salada, where HABs are reoccurring and the level of porewater nutrients was found to be highly elevated in the 2016 study (i.e., NH_4^+: 2,215; DON: 5,531, in $\mu mol \cdot L^{-1}$). Two pairs of shoreline nested piezometers were installed along a transect perpendicular to the shoreline. Porewater and surface water samples were collected along the transects extending offshore to approximately 200 ft from the shoreline. Monthly samples were collected for nutrient concentrations and stable isotopes and submarine groundwater discharge rates (SGD) were measured near the shoreline at the two locations. Nutrient sources and input mechanisms were evaluated and used to develop a water and nutrient mass balance. The results of this study will pave the way to a greater understanding of nutrients sources to Texas estuaries, an important step in meeting the overarching goal of the Coastal Zone Act Reauthorization Amendments (CZARA or §6217) to "protect coastal waters" by "control" of NPS pollution. The results are a step forward in the development and implementation of management measures leading to better control of nonpoint pollution sources and improved water budgets.

Submarine Groundwater Discharge

In the estuarine and coastal ocean setting, groundwater can be a significant source of inorganic N to local ecosystems and may provide up to 30% of the non-recycled N in the nutrient budget (Chaillou et al., 2014; Matson, 1993; Paerl, 1997). Giblin and Gaines (1990) found that N inputs from groundwater were similar in magnitude to riverine inputs in a river-dominated estuary. In bays with limited freshwater inflows and poor connection to a larger body of water, or rainfall that is significantly less than the local evaporation rate, submarine groundwater discharge (SGD) could influence the salinity of the local environment (Jolly et al., 2008) in addition to being an important source of nutrients. SGD, as described by (Moore, 2010), is "any and all flow of water on continental margins from the seabed to the coastal ocean, with scale lengths of meters to kilometers, regardless of fluid composition or driving force." Thus, SGD includes terrestrial groundwater and recirculated seawater (Santos et al., 2012).

Semi-arid estuarine systems are in general characterized by longer residence times, due to limited riverine inflows, and are known to cycle N for prolonged periods of time. In the absence of nutrient inputs from surface runoff, SGD could control primary productivity and lead to excessive algal growth or harmful algal blooms, especially in systems with long residence times (Hu et al., 2006; Jolly et al., 2008; Kroeger et al., 2007). In addition, even under low magnitudes of groundwater input, recirculated seawater can be a significant source of nutrients and anoxic waters to the water column (Santos et al., 2012). Development of anoxic conditions in the porewater could lead to the buildup of ammonium (NH_4^+) (Prokopenko et al., 2011; Schulz et al., 1994) that, later, can be released to the water column through SGD (including both groundwater and recirculated seawater) (Brock, 2001; Moore, 1996a). Increasing salinity levels in porewater is also very common in semi-arid estuaries (Bighash and Murgulet, 2015). Previous studies

indicate that salinity levels affect the N cycle of estuaries (Conley et al., 2009; Giblin and Gaines, 1990; Holmes et al., 2000). For instance, NH_4^+ release from sediment is dependent on salinity, with lower salinities effectively storing NH_4^+ in sediments and higher salinities releasing NH_4^+, which may enhance summertime primary production (Giblin et al., 2010; Holmes et al., 2000). The extent of SGD input is not fully known, but given the high enrichment of porewater and groundwater in nutrients, it is recognized to play a significant role in coastal ocean chemistry, even when volumetric inputs are low (Krest et al., 2000; Santos et al., 2012).

Nitrogen Cycling and Salinity

Nitrogen nutrients have a number of different forms, such as nitrite (NO_2^-), nitrate (NO_3^-), ammonia (NH_3), and ammonium (NH_4^+). Nitrogen enters estuarine systems through a variety of pathways including: atmospheric deposition, surface runoff (land and riverine), biological fixation, remineralization of decaying organic matter, and SGD (

Figure 1) (Fowler et al., 2013; Paerl, 1997; Santos et al., 2012; WSDE, 2017).

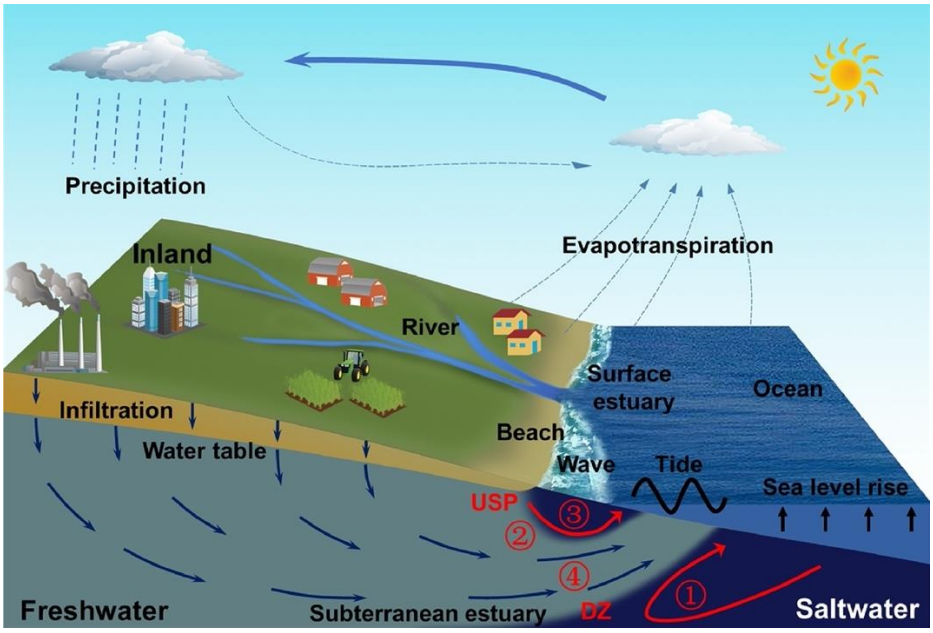

Figure 1: Conceptual diagram showing the interaction between a coastal unconfined aquifer and surface water including major flow processes: (1) density-driven recirculation, (2) tide-induced recirculation, (3) wave-driven recirculation and (4) terrestrial fresh groundwater discharge. The

subterranean estuary (STE) is associated with the dispersion zone (DZ) of the saltwater wedge and the upper saline plume (USP); from **Robinson et al. (2018)**.

In marine environments, processes that control the fate of bioavailable N can be affected by many factors including salinity (Conley et al., 2009). Nitrogen cycling mechanisms are interrupted in estuaries that can change from fresh to saline conditions (Conley et al., 2009; Jolly et al., 2008). As discussed by Jolly et al. (2008), many bays and estuaries in semi-arid regions are beginning to become hypersaline, and reverse estuaries are more common for some parts of the year. This change from a normal salinity, less than average ocean water (i.e., 35), to a hypersaline environment will influence the ecology of the bay or estuary as described above, including its ability to cycle nutrients (Conley et al., 2009). Such conditions occur in south Texas estuaries, like Baffin Bay, where drought conditions contribute to depletion of freshwater inflows from riverine sources leading to increased salinity surface waters (Schmidt and Garland 2012). Baffin Bay is often considered a reverse estuary (i.e., more saline than the bay it drains into) due to limited freshwater inflows from surface runoff, high evaporation rates, and limited connection with the Gulf of Mexico, which result in long residence times, greater than 1 year, and extreme salinities, up to 75-85 (Behrens, 1966; Folk and Siedlecka, 1974; Wetz et al., 2017). The bay is considered a schizohaline environment in that it changes from freshwater salinities to hypersaline conditions repeatedly over time (Folk and Siedlecka, 1974), as observed in Baffin Bay, but not during our investigation. Given Baffin Bay's long residence times and prolonged hypersaline conditions, forces on nutrient cycling and the effects of SGD can be observed. Baffin Bay has previously experienced a harmful algal bloom that lasted eight years, making it an area where understanding sources and cycling of nutrients is very important (Buskey et al., 2001).

Nitrogen Sources

These nutrient inputs in the form of DIN (i.e., NO_2^-, NO_3^-, NH_4^+) and DON enter the bay through runoff, riverine input, seawater recirculation/benthic fluxes, groundwater, and atmospheric deposition and are a vital source of nutrients to coastal water bodies. However, excessive nitrogen loading can dramatically alter these ecosystems and lead to various detrimental effects including eutrophication, hypoxia, fish kills and loss of biodiversity (Scavia and Bricker, 2006). Primary DIN and DON sources to Baffin Bay are sewage, livestock waste, fertilizer, atmospheric deposition but the contribution of each source to the excess nitrogen levels in the bay are unknown.

An approach to estimating source apportionment and determining processing of nutrients in coastal ecosystems is to characterize their stable nitrogen isotopic composition. Nitrogen exists in nature as nitrogen stable isotopes with a mass of 14 atomic mass units (^{14}N) and a mass of 15 amu (^{15}N). Due to this mass difference, different sources of nutrients have differing ratios of ^{15}N:^{14}N (reported as $\delta^{15}N$ values in permil (‰) units), and these different ratios act as a fingerprint for the distinct sources. For example, the $\delta^{15}N$ values of DON for the primary sources local to Baffin Bay are sewage (+23.6 ± 3.9‰), livestock waste (+3.9 ± 0.4‰), fertilizer (-0.6 ± 0.3‰), atmospheric deposition (+4.4 ± 0.3‰). Nutrient processing mechanisms also have unique isotope ratio effects associated with them. For instance, organisms such as *Aureoumbra lagunensis* tend to preferentially use the lighter isotope of nitrogen (14N) when assimilating nutrients for growth and energy. This leads to a change in the ^{15}N:^{14}N ratio of the nutrient pool which allows insight to how the nutrients are processed. This approach has been used extensively to investigate inorganic nitrogen (NO_3^-, NH_4^+) sources and processing in estuaries, bays, oceans and rivers (Sigman et al., 2009) and recent advances in isotope instrumentation and analysis

methods have allowed for isotopic studies investigating the lesser characterized nitrogen species, DON (Hadas et al., 2009; Knapp et al., 2005b; Tsunogai et al., 2008a; Wells and Eyre, 2019)**.** Since DON is the most abundant form of nitrogen (>90% of total N) in Baffin Bay, these advanced approaches are ideally suited to investigate nitrogen dynamics in the Bay.

Purpose

The extent of groundwater input and its role in releasing nutrients of terrestrial or remineralized origin is not fully understood in estuaries experiencing limited surface runoff, high evaporation rates and hypersaline conditions for most of the year. Since nutrient cycling rates and bioavailability are highly influenced by flushing rates (i.e., surface or subsurface runoff) and salinity levels, among other factors, it is important to understand the role SGD plays as a source of nutrients of terrestrial or remineralized origin. The relative abundances of different nutrients in and their sources in groundwater, bay and porewater were examined to evaluate sources such as fertilizers, atmospheric deposition, and septic/sewage. This study's main objectives were to determine and quantify the sources and processing of nutrients to the Laguna Salada arm of Baffin Bay.

Study Area

Baffin Bay is a shallow, well-mixed, semi-enclosed estuary located in southern Texas, bordered by Kleberg County to the north and Kennedy County to the south, on the Texas coastal plain in the northwestern Gulf of Mexico (**Figure 2**) (Dalrymple, 1964; Simms et al., 2010). The bay has a dendritic shape with three small arms branching off: Alazan Bay to the northeast, Cayo del Grullo in the northwest, and Laguna Salada in the southwest. The estuary provides essential habitat for numerous commercially and recreationally important marine species. The predominantly undeveloped land use surrounding Baffin Bay results in more pristine conditions

compared to other estuaries to the north. However, there are emerging concerns that the ecological health of this vital habitat is threatened by water quality degradation, specifically pertaining to persistent brown tides (Wetz et al., 2017).

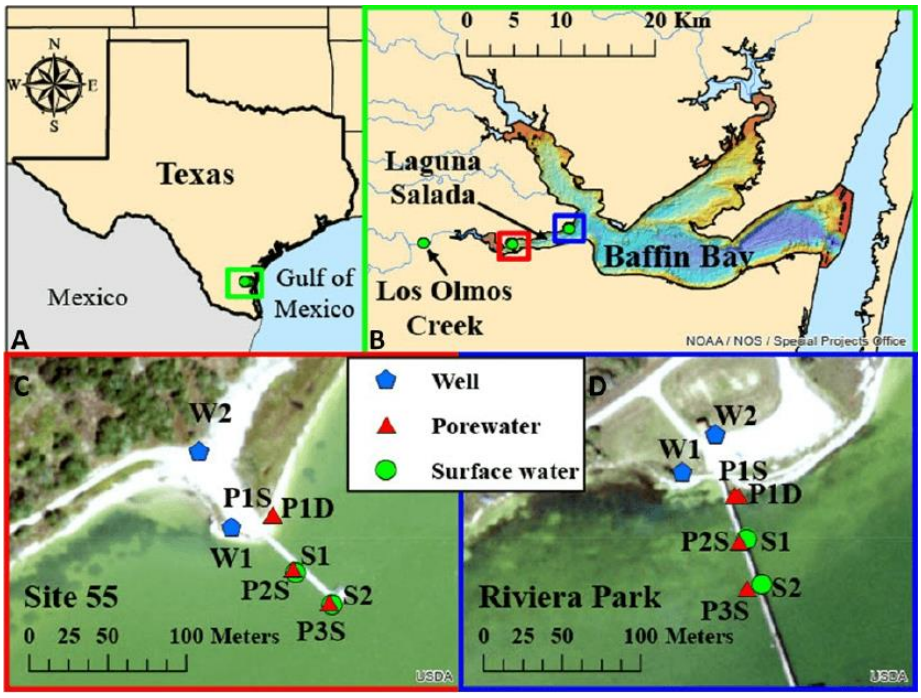

Figure 2: Study area location map including: the land use and land cover data for the Baffin Bay surroundings sampling stations. (A) Baffin Bay within Texas located along the south Texas coast; (B) Two sample locations along Laguna Salada and one at Los Olmos Creek. Los Olmos Creek feeds Laguna Salada. Laguna Salada is one of three fingers that comprise Baffin Bay; (C) Pore- (P), surface- (S), and groundwater (W) sample locations at site 55 (LS); (D) Pore- (P), surface- (S), and ground- water (W) sample locations at Riviera Park (RP).

The Coastal Plain gradient is very gentle, approximately 0.8 $m \cdot km^{-1}$ in the area of Baffin Bay (Simms et al., 2010), leading to low land runoff and likely high infiltration rates into soils and recharge to the water table aquifer (Fetter, 2001). The shoreline in the upper reaches of Baffin Bay consists of bluffs 2 to 4m high that grade down to tidal flats along the lower portion of the shoreline (Simms et al., 2010). Baffin Bay is isolated from the Gulf of Mexico by the 180 km long Padre Island and is further insulated from the contiguous Laguna Madre System by shallow reefs at the mouth of the bay (Simms et al., 2010). The nearest inlets that allow for

exchange between Baffin Bay and the Gulf of Mexico are Packery Channel and Aransas Pass (~41 km and ~70 km north of Baffin Bay, respectively) and Port Mansfield (~80 km south) (Wetz et al., 2017). Three creeks feed Baffin Bay: the San Fernando flowing into Cayo del Grullo, the Petronila flowing into Alazan Bay, and the Los Olmos into Laguna Salada. These creeks are believed to have carved the valley that now forms Baffin Bay in response to the last sea level drop at 20 ka (Behrens, 1963; Fisk, 1959; Simms et al., 2010). Los Olmos Creek, depicted in Figure 2 below, is the source of surface runoff to Laguna Salada and relevant to this project.

The semi-arid area of south Texas is characterized by high evaporation rates that exceed precipitation (60-80 $cm \cdot yr^{-1}$) by 60 cm annually (Behrens, 1966). This leads to average salinities of 40-50 and extremes as high as 85 during droughts and as low as 2 during large precipitation events (Behrens, 1966; Simms et al., 2010). Streamflow discharge data to Baffin Bay from its tributaries is limited; however, the freshwater inflow to and from the creeks is infrequent, thus contributing to the generally high salinities and long residence times (**Figure 3**). Data from 1967-2021 (collected approximately 40km inland from the bay) indicates that the Los Olmos Creek discharges on average 0.07 $m^3 \cdot s^{-1}$ (min: 0 $m^3 \cdot s^{-1}$, max: 37.66 $m^3 \cdot s^{-1}$) (USGS, 2021b). From 1965 to 2021 (collected from a stream gauge approximately 60 km inland from the bay), there was an average discharge of 0.42 $m^3 \cdot s^{-1}$ (min: 0.00 $m^3 \cdot s^{-1}$, max: 302.99 $m^3 \cdot s^{-1}$) from the San Fernando Creek (USGS, 2021a). From 2018 to 2020 (collected from a stream gauge approximately 25 km inland from the bay) the Petronila Creek discharged on average 0.79 $m^3 \cdot s^{-1}$ (min: 0.00 $m^3 \cdot s^{-1}$, max: 47.57 $m^3 \cdot s^{-1}$) (USGS, 2021c). No data up to 2021 are available for Petronila Creek.

The major sediment types found in Baffin Bay are black-mud, ooids, quartz-mollusk sands, and coated grains (Alaniz and Goodwin, 1974; Dalrymple, 1964). There are five major depositional environments found in Baffin Bay that differentiate it from other northern Gulf of Mexico bays: well-laminated carbonate and siliciclastic open-bay muds, ooid beaches, shelly internal spits and barrier islands, serpulid worm tube reefs, and prograding upper-bay mudflats (Simms et al., 2010). Sediment transport to Baffin Bay is limited to intense precipitation events by modern aeolian dunes, especially along the south shore (Simms et al., 2010). The dry climate caused an increase in $CaCO_3$ deposition in the soil in this area when compared to that northeast of Baffin Bay. Calcite formation around the shoreline acts as a shoreline stabilizer (Behrens, 1963; Driese et al., 2005; Price, 1936) that allows Baffin Bay to retain its dendritic shape (Behrens, 1963).

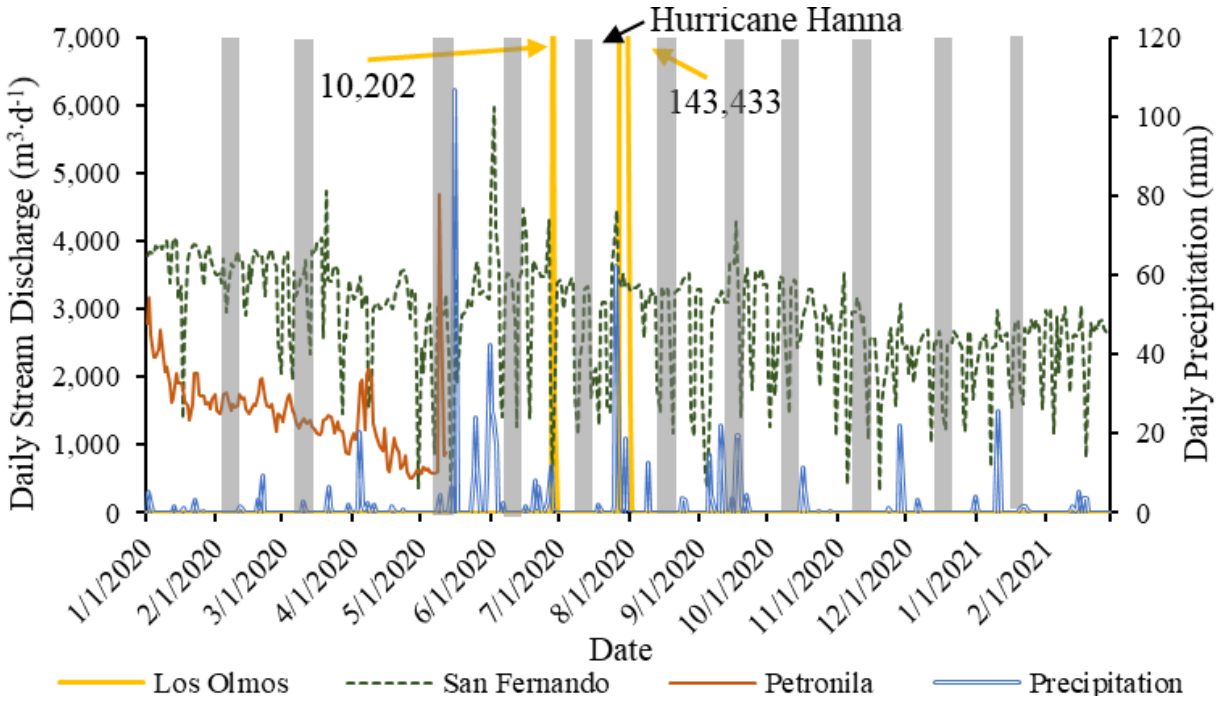

Figure 3: Precipitation (mm), discharge from San Fernando Creek, Petronila Creek, and Los Olmos Creek (USGS, 2017a, b) plotted for the duration of the study. The gray semi-transparent columns represent the time over which samples were collected. Note that there was not streamflow discharge from Los Olmos Creek except for 2 events that are likely to be outliers from equipment malfunction.

The Gulf Coast Aquifer (GCA) is a leaky artesian aquifer comprised of a complex of clays, silts, sands, and gravels (Ashworth and Hopkins, 1995) that form the Chicot, Evangeline, and Jasper aquifers (Waterstone and Parsons, 2003). The Baffin Bay estuary and the surrounding systems are generally in direct contact with the Chicot aquifer, which is the shallowest of the mentioned aquifers. The stratigraphic units of the Chicot aquifer consist of an overlying alluvial formation preceded by Beaumont and Lissie formations (Ashworth and Hopkins, 1995), which are generally composed of clays and clayey silts with intermittent sand and gravel lenses that continue out into the Gulf of Mexico (Waterstone and Parsons, 2003). The maximum total sand thickness of the GCA ranges from 700 ft in the south to 1,300 ft in the north with an average freshwater saturated thickness of about 1,000 ft (George et al., 2011). Brackish groundwater is more common than fresh groundwater in the southern GCA where water quality declines and total dissolved solids of 1,000 $mg \cdot L^{-1}$ or more are common (George et al., 2011).

In general, within the coastal aquifer, groundwater flows toward the coast, eventually discharging into the bays and estuaries. Nevertheless, the watersheds surrounding Baffin Bay receive significantly less precipitation than systems further north and there is a significant drawdown around Kingsville that may inhibit groundwater flow from confined hydrostratigraphic units toward the coast. Strong southeast winds of 16 to 32 km per hour ($km \cdot h^{-1}$) are dominant from February to August (Dalrymple, 1964; Rusnak, 1960); however, from September to February, the dominant wind direction shifts to the northwest with an average speed of 18.35 $km \cdot h^{-1}$ (Lohse, 1955; TCOON, 2016). Baffin Bay is a shallow estuary with an average depth of 2 m (max: 3 m) (Simms et al., 2010) that experiences only small astronomical tides (<0.1 m) (Simms et al., 2010). With the strong, persistent winds and shallow depths, the

tides are mainly controlled by wind and precipitation events (Breuer, 1957; Militello, 1998). Consequently, the bay is generally well-mixed with little stratification under normal conditions.

A previous study in Baffin Bay ranked, from largest to smallest, the sources of external N to the system as: 1) atmospheric deposition, 2) fertilizer, 3) manure from livestock, 4) urban runoff from developed land, and 5) industrial and municipal point sources (Rebich et al., 2011). This study did not account for groundwater although it has been shown to be a likely contributor of external N to the bay (Breier et al., 2010; Santos et al., 2012; Uddameri et al., 2013). The relative contributions of each source are dependent on hydroclimatic conditions and thus are expected to shift with changes in precipitation and return flows. For instance, during drought conditions some of the tributaries often run dry while others, such as the San Fernando Creek, which has 12 permitted wastewater facilities and likely is dominated by point source N (Wetz et al., 2017), flow perpetually and could contribute a continuous source of N and other forms of nutrients.

METHODS

Water Sample Collection

Aqueous samples were collected monthly for a year from groundwater (from 4 monitoring wells), surface water and porewater during the radon time series events at the Riviera Park and Site 55, in Laguna Salada (Figure 2). In general, surface water samples were collected at each of the two locations, at the beginning, mid, and end of the time series. The water depth at the intake for surface water samples and radon monitoring was measured using a pre-labeled line attached to a weight. Samples from the water column were collected to 0.2m below air-water interface. Field parameters were measured before sample collection using an YSI multiparameter water quality meter. The YSI meter was placed at each sampling depth within the water column for several minutes to allow proper circulation of sample and instrument stability before parameters were recorded.

Surface water samples were collected with a Van Dorn bottle deployed to the desired depth and given a few minutes to allow water to circulate through the cartridge, according to standard operating procedure (TCEQ, 2012). All sampling bottles were rinsed three times and then overfilled, capped, and placed on ice, depending on the required procedure for each analyte. For dissolved gas samples (i.e., ^{222}Rn) a rubber tube was used to transfer the sample with minimal air exposure. Porewater was collected at each site at two locations along the transect by inserting a push-tip piezometer (AMS Retract-a-Tip) connected through silicone tubing to a peristaltic pump about 0.13 to 1.0 m below the sediment-water interface (i.e., deep enough to prevent bottom waters from contaminating porewater sample (RCRA SOP, 2009)). Before sample collection, the tubing was flushed until the sample was clear (or a minimum amount of

sediment was present in the sample) and the field parameters (i.e., salinity, temperature, pH) stabilized.

All porewater and groundwater samples for ^{222}Rn analysis were collected in 250 mL gas-tight borosilicate bottles filled from the bottom and allowed to overflow for one volume before being sealed with no headspace. Measurements of ^{222}Rn were conducted with a Durridge RAD-7 following the WAT250 protocol (Durridge Company Inc., 2017) within 2 days of sample collection to prevent loss due to decay (half-life 3.8 days) and decay corrected to time of sampling. Surface water samples from Los Olmos Creek or offshore surface water were collected in 2L bottles and ^{222}Rn was measured using the Durridge RAD7 radon-in-air monitor with the soda bottle accessories and protocols (Lee and Kim, 2006).

Nutrient

Water samples were collected in acid-washed amber polycarbonate bottles using the techniques mentioned above. Bottles were stored on ice until return to a shore-based facility where processing of samples occurred, and analyses were conducted nutrients and organic matter (surface water and porewater).

Inorganic nutrients (nitrate (NO_3^-), nitrite (NO_2^-), ammonium (NH_4^+), orthophosphate (HPO_4^{2-}), silicate ($HSiO_3^-$)) were determined from the filtrate using a Seal QuAAtro autoanalyzer. The method detection limit was determined for each analyte and matrix by the EPA method detailed in 40 CFR Part 136, Appendix B. The method detection limit (MDL) is defined as the Student's t for 99% confidence level times the standard deviation of seven replicate measurements of the same low level sample or spiked sample. The applicable concentration ranges of this method are defined by the concentration range of the calibration solution adjusted by the estimated sample concentrations. If the sample concentration exceeds

the linear range, the sample was diluted and reanalyzed. The method detection limit (MDL) in µM for the nutrients are: 0.11for NO_3^-, 0.012 for NO_2^-, 0.057 for NH_4^+, 0.025 for HPO_4^{2-}, 0.14 for $HSiO_3^-$.

Ammonium Removal Procedure Before Total Dissolved Nitrogen Conversion for Isotope Analysis

Ammonium was removed before total dissolved nitrogen oxidation. Of each sample, 40 mL was added to 100 mL beakers. 5N NaOH was added to raise the pH which forces the ammonium/ammonia to volatilize. Beakers were then weighed and left uncovered in a fume hood under darkness. After 24 hours [NH_4^+] is checked via OPA method. Once the ammonia is no longer detectable, the beakers are carefully weighed. The difference in weights is used to determine the new concentrations due to water loss by evaporation. The reason ammonium is removed this way is to reduce systemic errors incurred while measuring the various concentrations, i.e., there is one less measured analyte concentration needed to calculate [DON] and δ^{15}N-DON.

Isotopic Analysis of Dissolved Inorganic Nitrogen

DIN ($NO_2^- + NO_3^- + NH_4^+$) isotopic composition was only able to be measured if DIN concentration were greater than 3 µM due to method and instrumentation limits. If NO_2^- accounted for more than 2% of the $NO_2^- + NO_3^-$ concentration, it was removed using sulfamic acid so the resulting δ^{15}N represented just the δ^{15}N-NO_3^- value (Granger and Sigman, 2009). Once isolated, NO_3^- was converted to N_2O via the denitrifying bacteria, *Pseudomonas aureofaciens*. The isotopic composition of NO_3^- was then determined as δ^{15}N-N_2O by injecting the N_2O into a continuous flow isotope ratio mass spectrometer (CF-IRMS) (Sigman et al., 2001). Internationally recognized standards (USGS34, USGS32, IAEA-N3 and USGS35) were

measured during sample analysis to provide a known $\delta^{15}N$ -NO_3^- reference for data corrections. Values are reported in parts per thousand, relative to atmospheric N_2 as follows:

$$\delta^{15}N\ (‰) = [(^{15}N/^{14}N_{sample}) - (^{15}N/^{14}N_{standard})] / (^{15}N/^{14}N_{sample}) * 1000 \quad (1)$$

Isotopic Analysis of Total Dissolved Nitrogen

After ammonium removal, TDN (NO_3^- + DON) of the samples was oxidized to NO_3^- using the persulfate method (Tsunogai et al., 2008b). The persulfate working reagent was prepared using ultrapure High-Performance Liquid Chromatography (HPLC) Grade water. The average blank concentration (14.23 µM ± 3.1 µM) was mainly attributed to reagent water and since a relatively small amount of persulfate working reagent (0.60 mL) is added to the Baffin Bay samples coupled with the fact that Baffin Bay is a high DON environment, the overall blank effect is minimal (average 2.4%). Representative DON standards (i.e., urea, glycine, N-acetyl-D-glucosamine) were oxidized along with the Baffin Bay samples monitor efficiency of TDN to NO_3^- from the persulfate oxidation. Resulting NO_3^- concentrations were measured via the cadmium reduction colorimetric method (APHA, 1992). Urea was chosen as a standard because it is a form of DON that is a common component used in fertilizers and has been shown to contribute approximately 50% of the N utilized in many coastal regions (Bronk, 2002). Glycine was chosen as a standard to represent the dissolved free amino acid (DFAA) portion of the DON pool, which has been found to comprise approximately 1.2 to 12.5% of the total DON pool (Bronk, 2002). The N-acetyl-D-glucosamine was chosen as a standard because studies have shown that this biopolymer is representative of the N-acetyl amino polysaccharides (N-AAPs) and are important contributors to the semi-labile pool of DON (NAAPs can comprise ~40 to 50% of surface ocean high molecular weight dissolved organic matter (HMWDOM) (Aluwihare et al., 2005). Once the TDN in the sample was converted to the NO_3^- the isotopic composition

was measured via the denitrifier method described above (Knapp et al., 2005a; Knapp et al., 2011a; Sigman et al., 2001). The δ^{15}N-DON value was calculated from the measured δ^{15}N-NO_3^- and δ^{15}N-TDN by using the isotope mass balance equation:

$$\delta^{15}\text{N-TDN} = f_{NO3-}(\delta^{15}\text{N-NO}_3^-) + f_{DON}(\delta^{15}\text{N-DON}) \quad (2)$$

where f_{NO3-} and f_{DON} stands for the fraction of the concentration of the respective DIN/DON contributing to the TDN concentration of the samples.

Isotope Mixing Model (DON Source Apportionment)

Nitrogen source contributions can be estimated using an isotope mixing model if the isotopic compositions of the primary nitrogen sources are known and the isotopic composition of nitrogen in a sample has been measured. For this project, a four-end member isotope mixing model was developed using source signatures of four primary sources (i.e., septic/sewage, livestock waste, fertilizer, and wet atmospheric deposition) and the measured isotopic composition of DON in Baffin Bay samples (equ 3). Table 1 includes the literature δ^{15}N-DON values of DON sources and the δ^{15}N-DON values of local sources used in the mixing model (Campbell, 2018). The δ^{15}N-DON value from septic/sewage is adjusted with wastewater outfall value from reference and measured δ^{15}N-DON in the well samples from the transect assuming the primary DON source in this location is the septic field. The SIAR package was used to employ the mixing model. The SIAR is an R package based on Bayesian statistical method. The Bayesian statistical method can account for variations in fractionation factors, integrate uncertainties and use prior information to guide analyses (Moore and Semmens, 2008; Parnell et al., 2010; Parnell et al., 2013). The names, mean isotopic compositions and standard deviations of DON sources were entered in the R code along with the δ^{15}N-DON value of surface water

samples. SIAR provides the best estimated mean contribution of each sources and corresponding uncertainty.

$$\delta^{15}\text{N-DON}_{bay} = f_{ss}(\delta^{15}\text{N-DON}_{ss}) + f_{wad}(\delta^{15}\text{N-DON}_{wad}) + f_{fert}(\delta^{15}\text{N-DON}_{fert}) + f_{lw}(\delta^{15}\text{N-DON}_{lw}) \quad (3)$$

Where $\delta^{15}\text{N-DON}_{bay}$ is of the δ^{15}N value of the bay sample, f_{ss} is the contribution of septic/sewage, $\delta^{15}\text{N-DON}_{ss}$ is the δ^{15}N value of septic/sewage, fwad is the contribution of wet atmospheric deposition, $\delta^{15}\text{N-DON}_{wad}$ is the δ^{15}N value of wet atmospheric deposition, f_{fert} is the contribution of fertilizer, $\delta^{15}\text{N-DON}_{fert}$ is the δ^{15}N value of fertilizer, f_{lw} is the contribution of livestock waste and $\delta^{15}\text{N-DON}_{lw}$ is the δ^{15}N value of livestock waste.

Table 1: δ^{15}N values of reported DON sources and local DON sources. Local livestock waste is δ^{15}N-TDN (Campbell, 2018; Choi et al., 2017; Cornell et al., 1995; Curt et al., 2004; Lee et al., 2012; Russell et al., 1998). *Local value from Campbell 2018 and local septic included from this study's well samples.

DON Source	Literature δ^{15}N value (‰)	*Local δ^{15}N value (‰)
Septic/Sewage	+12.8 to +18.6	+23.6 ± 3.9
Wet atmospheric deposition	-7.9 to +7.0	+4.4 ± 0.3
Synthetic organic fertilizer	-6 to +2	-0.6 ± 0.3
Livestock waste	+3 to +14	+3.9 ± 0.4

Submarine Groundwater Discharge Estimates

SGD rates were calculated using Darcy's law, time-series ^{222}Rn, and radium activities, as described below.

Darcy Discharge Rate Estimates

Darcy's law estimates of groundwater velocity (v, Darcy's Law formulas below) of "local" shallow, brackish to hypersaline SGD were derived using water level and hydraulic conductivity data from the four groundwater monitoring wells located near the monitoring sites (Figure 2). Following well installation at the beginning of the project, standard slug-in tests with the

Hvorslev method (1951) were conducted at the monitoring wells with a pressure data logger collecting data at 1 Hz to estimate horizontal hydraulic conductivity of the shallow aquifer sediments. The pressure transducers were set to correct for density, dependent on each groundwater characteristics at each well.

$Q = K \cdot i \cdot A$ and $v = K \cdot i/n$; where K is the hydraulic conductivity, i is the hydraulic gradient, A is the cross-sectional area to flow; v is seepage velocity and n is effective porosity.

Radiogenic Isotopes Rate Estimates

Radium mass balance and SGD Rates

Samples for radium (radium-223 [^{223}Ra], radium-224 [^{224}Ra], radium-226 [^{226}Ra]) analysis were collected in three-20L jugs (approximately 45 to 60 L total volume) at each of the two sampling sites using a sump pump positioned ~0.2 m above the sediment-water interface. The radium was extracted by processing the samples through ~15g manganese dioxide, MnO_2, impregnated acrylic fibers two times at a flow rate <1 $L \cdot min^{-1}$ (Dimova et al., 2007; Kim et al., 2001). The Mn-fibers were then rinsed thoroughly with Ra-free water to eliminate any salts or particulates and then pressed to a water to fiber ration of 0.3-1g (i.e. 20-30g wet weight) (Sun and Torgersen, 1998). The fibers were tested for ^{223}Ra (half-life: 11.4 days) and ^{224}Ra (half-life: 3.6 days) on a Radium Delayed Coincidence Counter (RaDeCC). Activities of ^{224}Ra were measured within three days of collection given the short half-life (Moore, 2006). After the short-lived isotope measurements, the fibers were flushed with nitrogen gas and sealed for >21 days to reach secular equilibrium before measuring the ^{226}Ra (half-life: 1,600 years) on a RAD-7 with measurements corrected to a calibration curve determined from 5 standards (Moore, 1996a).

Radium-based SGD estimates, representative of the portion of the bay where measurements were conducted (Charette et al., 2001), were determined using a radium mass balance approach. Radium apparent age (T_r) is an essential term in the radium mass, and

although not direct measurements of bay residence times, they are an indicator of how fast water moves through the porous media (Swarzenski et al., 2007). Relative radium apparent ages of the surface water represent the relative time that has passed since Ra first entered a well-mixed estuary, and therefore has been separated from its radionuclide source (i.e., subsurface sediments). They were calculated using the activity ratio (AR) of the short-lived ^{224}Ra ($t_{½}$ = 3.66 days) to the longer-lived ^{223}Ra ($t_{½}$ = 11.4 days) and ^{226}Ra ($t_{½}$ = 1,600 yr) isotope, i.e., equation 4, following the steps described in numerous previous studies (Dulaiova and Burnett, 2008; Knee et al., 2011; Moore, 2000a).

$$T_r = \frac{AR_{GW} - AR_{CO}}{AR_{CO} \times \lambda_{224}} \quad (4)$$

where AR_{GW} is the initial activity ratio of the discharging groundwater source, AR_{CO} is the measured activity ratio of the surface water at the station of interest, and λ_{224} is the decay constant (d^{-1}) for the short-lived ^{224}Ra isotope.

A mass balance was developed for each location to determine the excess ^{226}Ra and ^{223}Ra (due to groundwater flux) in the bay. Briefly, this includes all sources of radium other than groundwater, including tidal exchange, riverine dissolved input (where applicable), desorption from riverine suspended sediments, and decay (i.e., ^{223}Ra). The mathematical expression and detailed explanation of terms are found in Moore (1996b) and (Lopez et al., 2020). Expressed mathematically, excess ^{226}Ra ($^{226}Ra_{ex}$ [Bq·d^{-1}]) or excess ^{223}Ra ($^{223}Ra_{ex}$ [Bq·d^{-1}]) in the bay equals:

$$Ra_{ex} = \left[\frac{(Ra_{BB} - Ra_{Sea})V_{bay}}{T_r}\right] - [Ra_r Q_r] - [Ra_{des} Q_r] + [(1 - e^{\lambda T_r})V_{Bay}] \quad (5)$$

where Ra_{BB} is the average measured ^{226}Ra or ^{223}Ra activity in the bay; Ra_{sea} is the average ^{226}Ra or ^{223}Ra activity in the offshore water body (i.e., Laguna Madre in the case of Baffin Bay), which exchanges tidally with the bay of interest; Ra_r is the average ^{226}Ra or ^{223}Ra activity from rivers

and streams, Ra_{des} is the average ^{226}Ra or ^{223}Ra activity from desorption experiments, Q_r is the average stream discharge, V_{bay} is the volume of the bay of interest; T_r is the residence time, or flushing rate, estimated from the apparent radium water ages (i.e., equation 4).

Endmembers for offshore or tidal influence were selected from previous projects (Douglas et al., 2020; Lopez et al., 2020; Spalt et al., 2019) or from the lowest activity sample in a time series, which acts as a background activity level, providing a conservative excess radium measurement, similar to Peterson et al. (2008). Specific to this study, desorption laboratory experiments from sediment cores, conducted following the experimental setup by Sadat-Noori et al. (2016), collected at each location showed that the dissolved ^{226}Ra and ^{223}Ra fluxes from bottom sediments alone ($\bar{x}$: 1.2 $dpm \cdot m^{-2} \cdot d^{-1}$ and $1.9x10^{-4}$ $dpm \cdot m^{-2} \cdot d^{-1}$, respectively) were negligible. This agrees with other studies that excluded sediment desorption from the ^{226}Ra and ^{223}Ra mass balance (Beck et al., 2007; Beck et al., 2008; Lopez et al., 2020; Moore, 2000b; Sadat-Noori et al., 2016; Tait et al., 2017). For radium input from riverine discharge, radium desorption experiments were conducted using riverbed sediment samples (i.e., 0 -10 cm) from the freshwater portion of bay tributaries. Bay water samples, of salinities 20 and 30, were filtered through Whatman GF/F filters to remove suspended solids and processed as described by Lopez et al. (2020) and references therein (Gonneea et al., 2008; Ward and Armstrong, 1997). Riverine contributions of ^{226}Ra, or ^{223}Ra, were determined by normalizing the total activity to the sediment mass, multiplied by the respective season tributaries sediment flux from USGS and Texas Water Development Board's (TWDB) modeled freshwater inflows (TWDB, 2019a, b, c; USGS, 2019a, b). The TWDB modelled inflows include the ephemeral creek discharges, surface runoff, and return flows to the creeks. The decay rate of ^{226}Ra was neglected, given that its half-life is much longer with respect to the bay mixing time. On the other hand, the model accounts

for decay rate of ^{223}Ra, due to its much shorter half-life.

The excess activity from the mass balance is assumed to be the result of SGD. Using the porewater endmember activity (Ra_{PW}) for ^{226}Ra or ^{223}Ra at each location for the corresponding season, SGD is calculated from:

$$SGD_{Ra} = \frac{Ra_{ex}}{Ra_{PW}} \quad (6)$$

Douglas et al. (2020) and Lopez et al. (2020), found that SGD estimates using both porewater and groundwater endmembers were in close agreement, but seasonal fluctuations in porewater radium activities need to be accounted for. Porewater geochemical characteristics reflect mixing of terrestrial and marine (i.e., recirculated seawater) sources and any deep groundwater short-lived radium isotope would approach equilibrium with near surface sediments before entering surface water (Knee et al., 2011). Thus, they are likely the most representative endmember.

Radon mass balance and SGD Rates

Stationary time series measurements of ^{222}Rn were used to construct a mass balance and inventory as described in detail by Burnett and Dulaiova (2003); Lambert and Burnett (2003); Smith and Robbins (2012), and references therein. The inventory of ^{222}Rn over time allows for an evaluation of losses/gains due to mixing with waters of different ^{222}Rn activities (i.e., depleted offshore waters), atmospheric evasion, and sediment inputs. Therefore, changes over time, if any, are used to determine ^{222}Rn fluxes (F_{total}) as shown in equation 4. Water fluxes (cm·d^{-1}) were estimated by dividing ^{222}Rn fluxes by the ^{222}Rn activity of the advective groundwater fluids ($^{222}Rn_{gw}$) (Burnett and Dulaiova, 2003), as shown below:

$$SGD = \frac{F_{total}}{^{222}Rn_{gw}} = \frac{[z(A_{Rn} - \lambda_{222}A_{Ra})] + F_o - F_i - F_{sed} + F_{atm} \pm F_{mix}}{^{222}Rn_{gw}} \quad (7)$$

where A_{Rn} is the activity of ^{222}Rn in the water column, $\lambda_{222}A_{Ra}$ is the flux of ^{222}Rn due to production from dissolved ^{226}Ra in the water column, z is the water column depth, F_o is the

offshore flux (flood tide), F_i is the inshore/nearshore flux (ebb tide), F_{sed} is the sediment flux, F_{atm} is the losses due to atmospheric evasion, and F_{mix} is the losses due to mixing processes. Using the total flux (F_{total}) and the excess ^{222}Rn of the advective fluids ($^{222}Rn_{GW}$), which in this study is the activity of ^{222}Rn in groundwater, ^{222}Rn fluxes (F_{total}) are converted to SGD as in equation 3.

Although short term tidal fluctuations are insignificant in this area (no more than 12 cm observed for the duration of time series at all sites and seasons), the mass balance accounts for any change in water level throughout the monitoring period from hourly measurements at the RAD7 intake. Offshore endmember selection during the time series has proven difficult given sudden changes in wind direction, thus, changes in direction of flow and endmember activity. For that reason, the maximum absolute values of the observed negative fluxes during each time-series event were used to correct ^{222}Rn fluxes for losses via mixing, after correction for atmospheric evasion. Given the persistent winds and the shallow nature of these systems, there are concerns that atmospheric evasion may not accurately be estimated by the ^{222}Rn mass-balance (Lopez et al., 2020; Spalt et al., 2018). To compensate for this, gas transfer velocities, were calculated using wind speeds for the day and the preceding two days of sampling (Rodellas et al., 2021).

Corrections for in-situ production of ^{222}Rn were done using surface water ^{226}Ra at high and low tides during each sampling event. Sediment-supported ^{222}Rn was derived from laboratory equilibration experiments using site-specific sediment cores (ranging in length from 21 to 59 cm, $\bar{x}$ core length 38.6 cm) as outlined by Corbett et al. (1998).

RESULTS AND DISCUSSION

Salinities

Overall surface water salinities were the lowest (e.g., 41) in February at RP and the highest (58) in July, also at RP, with an average of all seasons and locations of 47. Average salinities were only slightly higher in February than in March 2020 and continued to increase to 58 in July 2020 and slowly decreased to levels similar to spring. Salinities at both sites followed similar trends and were very similar until September when RP readings exceed those at LS and continue to be higher for the reminder of the monitoring period (Figure 4a).

Porewater salinities follow similar trends as surface water and groundwater. The magnitudes measured in porewater are similar to surface water at both sites except those at LS starting in June 2020. Beginning in June, salinities in porewater at LS exceeded those at RP and approach the LS groundwater. Porewater salinities were the lowest (e.g., 39) in March at RP and the highest (81) in August, at RP, with an average of all seasons and locations of 49.

Groundwater salinities measured in the four monitoring wells at the RP and LS sites showed large variabilities (Figure 4b), although located at the same depth (at each site) and only approximately 50 to 100 ft away from each other (Figure 2). The largest differences were observed at RP, where the well located slightly further inland (well 2) had salinities ranging between 5 and 12. On the other hand, the nearshore groundwater (well 1) exhibited salinities ranging from 48 to 88. At LS, the while differences between the two wells are still observed, both locations had salinities in the hypersaline range. The nearshore well (well 1) ranged between 65 and 82, while the further inland (well 2) salinities were between 51 and 63. The largest change in salinities among all four wells was observed at LS for well 1, nearshore, following Hurricane Hanna, with an increase from 61 in July (close to porewater) to 88 in

August. Following, salinities dropped to values lower than in July and continued to stay in that range for the reminder of the study. The observed differences in salinities among the four locations reflect the large subsurface heterogeneity in terms of aquifer physical properties and connection to the estuary. It is also indicative that near the shore in the investigated area, shallow groundwater inputs could be variable, but are likely to be predominantly hypersaline, which explains also the hypersaline nature of porewaters.

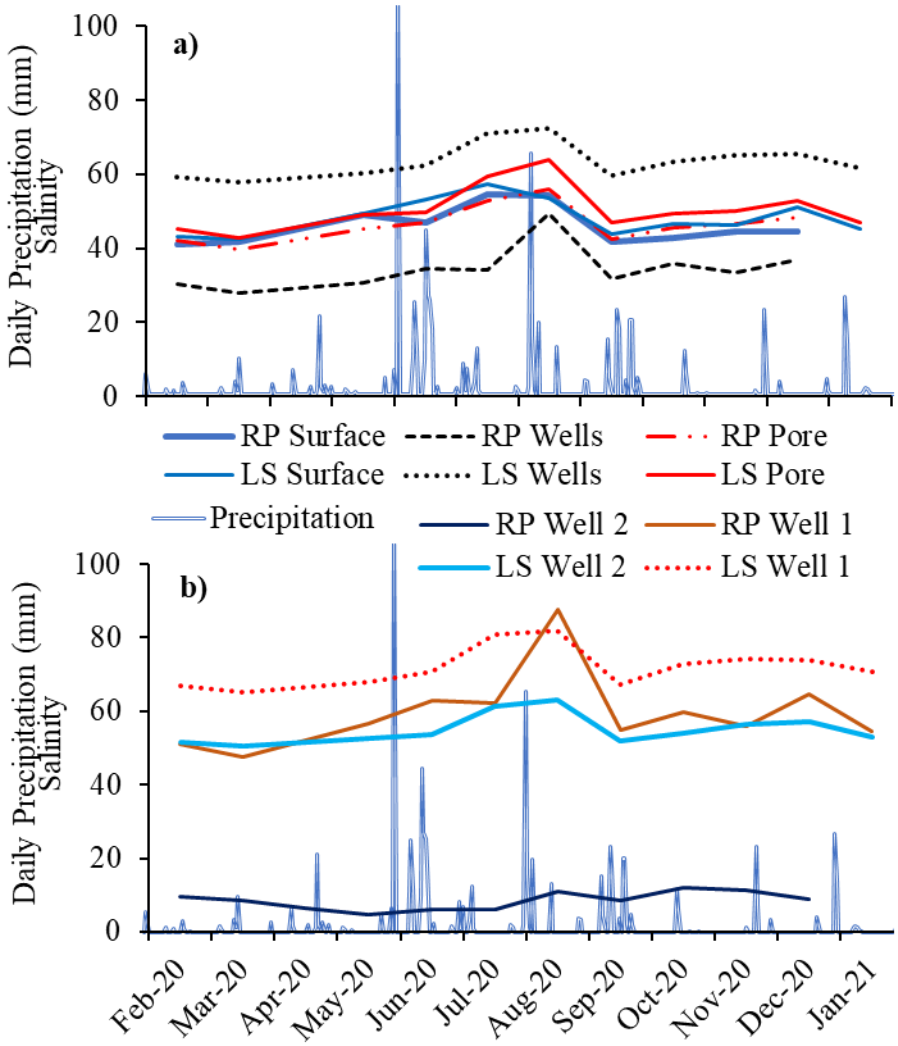

Figure 4. Salinity changes by site and type of sample (e.g., surface water, porewater, and groundwater-well) (a) and by well for sites RP and LS.

Nutrients

Inorganic and Organic Nitrogen Concentrations and Isotopic Composition

Groundwater

Sampling was conducted across transects at both the RP and LS sites to explore temporal and spatial nitrogen dynamics in the surface water, porewater and groundwater (Figures 5-11). The average concentrations NH_4^+ concentrations at the RP site and LS site were 0.6 ± 1.1 and 489.4 ± 458.0 µM, respectively. The highest NH_4^+ concentration of groundwater observed at the RP site was 3.1 µM while the highest at LS of was 1041.7 µM. This difference in NH_4^+ concentration potentially reflects the physiographic characteristics of the area, like the presence of salt flats in the LS area because of the low elevation environment and frequently flooded with seawater at high tides, which infiltrates to the groundwater. Thus, groundwater near the shoreline at this location shows porewater like signatures, i.e., high NH_4^+ concentration. The RP site, which is more elevated (approximately 15 ft above mean sea level) did not show signs of flooding during sampling periods and had lower NH_4^+ concentration. This, however, could also be the results of different substrate characteristics, like more sandy substrates are more conductive and groundwater is usually more oxic, thus, the higher NO_3^- as observed in this study.

The RP site is near a septic system, where groundwater may be contaminated by the septic effluent discharge. The average DON concentrations at RP-W1 and RP-W2 were 23.3 ± 10.5 µM and 33.2 ± 18.7 µM, respectively (Figure 7). The average δ^{15}N-DON values at RP-W1 and RP-W2 were +21.6 ± 2.7‰ and +27.1 ± 1.8‰, respectively (Figure 11). This enriched δ^{15}N-DON indicates a septic source. Soil-based septic systems are commonly reliant on anaerobic environments which favor mineralization where organic nitrogen is ammonified leaving residual DON enriched in δ^{15}N (McGonigle et al., 2012; Möbius, 2013). When not all but a portion of

organic nitrogen is converted to NH_4^+, fractionation occurs. The fractionation during ammonification is small (-1.43‰ to -2.3‰) (Möbius, 2013), but DON derived from septic effluent can be highly enriched in $\delta^{15}N$ as considerable amounts of NH_4^+ are generated in this type of environment. Thus, the enriched $\delta^{15}N$-DON in groundwater suggests that a septic source may be the dominant source of DON at RP.

Septic effluent can percolate to the water table and be transported with groundwater to surface water (e.g., Baffin Bay). Septic effluent consists of a large portion of NH_4^+ (70 to 90%) but only a small amount of NO_3^- because of its anaerobic characteristics (Lusk et al., 2017). However, the groundwater at RP has an average NO_3^- concentration of 29.9 ± 8.1 µM and an NH_4^+ average of only 0.6 ± 1.1 µM (Figures 5, 6). This may be explained by nitrification of NH_4^+ that occurs as the septic effluent percolates to the water table within an oxic environment. Nitrification can oxidize NH_4^+ into NO_2^- or NO_3^-. This is indicated by the enriched $\delta^{15}N$-NH_4^+ of groundwater. Nitrification prefers to utilize light nitrogen, leaving the residual NH_4^+ enriched in $\delta^{15}N$. This scenario explains the enriched average of $\delta^{15}N$-NH_4^+ at RP-W1 and RP-W2 of +54.7 ± 41.5‰ and +43.1‰, respectively (Figure 8), which is much higher than the $\delta^{15}N$-NH_4^+ from human waste (+4.4 ± 4.6‰) (Nikolenko et al., 2018). Since NH_4^+ was nitrified, only 0.6 ± 1.2 µM of NH_4^+ is left in groundwater and continues to be transferred to porewater (Figure 5).

Based on observation in the nearby groundwater, mentioned above, nitrification of septic effluent is expected to be a major source of NO_3^- in porewater in the nearby bay. At RP-W1 and RP-W2, average NO_3^- concentrations were 29.7 ± 7.0 µM and 30.2 ± 10.2 µM, respectively (Figure 6). The average $\delta^{15}N$-NO_3^- of RP-W1 (16.5 ± 0.6‰) and RP-W2 (27.7 ± 3.9‰) are higher than the $\delta^{15}N$-NH_4^+ from human waste, which implies the presence of denitrification (Figure 9). Denitrification can convert NO_3^- into NO, N_2O or N_2 and preferentially uses the light

nitrogen, leaving the residual NO_3^- enriched in ^{15}N. The occurrence of denitrification in porewaters in the nearby RP area is also demonstrated through a plot of $\delta^{18}O\text{-}NO_3^-$ versus $\delta^{15}N\text{-}NO_3^-$ (Figure 12) where a strong linear relationships between $\delta^{18}O\text{-}NO_3^-$ and $\delta^{15}N\text{-}NO_3^-$ is observed. The denitrification process creates a proportional relationship between residual $\delta^{18}O\text{-}NO_3^-$ and $\delta^{15}N\text{-}NO_3^-$ and results in a linear relationship with slopes of ~1. RP-W1 showed a strong linear relationship and is close to a denitrification line of 1:1 while RP-W2 showed a similar relationship with a slope slightly less than 1. These trends have been observed in groundwater when denitrification occurs and can be explained by the anaerobic nitrification using oxidants other than O_2 or by the O exchange between NO_2^- and water and the oxidation of NO_2^-, which lowers the slope (Kendall et al., 2007). This indicates that nitrification and denitrification may be the two dominant processes contributing to the nitrogen and oxygen isotope composition in RP-W2. Both RP-W1 and RP-W2 show that the mixing process is insignificant, as demonstrated by the Keeling plots (Figure 13).

The LS site is located near underdeveloped agricultural and brushy land and is frequently flooded by surges. The average $\delta^{15}N\text{-}NH_4^+$ of LS-W1 and LS-W2 is 9.0 ± 3.4‰ and 7.8 ± 3.6‰, respectively (Figure 8). Both are close to the average $\delta^{15}N\text{-}NH_4^+$ (8.0 ± 5.5‰) of LS-porewater, signifying a close interaction between the two environments. Like porewater, the groundwater at LS site contains high concentrations of NH_4^+, up to 1041.7 µM (Figure 5), but lower than previously reported by Murgulet's study in 2016 in the more offshore areas of the bay (see Background and Relevance section). However, it is much higher than the porewater NH_4^+ concentration at this location (243.4 ± 118.0 µM). Here the mineralization of organic nitrogen is suspected to be another NH_4^+ source. The mineralization of organic nitrogen produces NH_4^+ and has an associated fractionation values ranging from -1.43‰ to -2.3‰ (Möbius, 2013). The

negative fractionation generates depleted $\delta^{15}N\text{-}NH_4^+$ compared to the $\delta^{15}N$ of reactant (e.g., DON) and leaves the residual DON reactant leading to offset between porewater NH_4^+ and porewater $\delta^{15}N$-DON (+14.3 ± 3.6‰) (Figure 11). A similar $\delta^{15}N$-DON in groundwater (16.6 ± 2.5‰) at the site could point to a similar mineralization effect which is expected due to the aforementioned physiographic characteristics of the well location being analogous to the porewater environment. Nevertheless, the generated $\delta^{15}N\text{-}NH_4^+$ was close to the $\delta^{15}N\text{-}NH_4^+$ of porewater and does significantly alter the value of $\delta^{15}N\text{-}NH_4^+$. The slightly lower DON concentration of groundwater (27.8 ± 13.5 µM) than porewater (34.1 ± 15.9 µM) at this site can also be explained by the mineralization process (Figure 7). The NO_3^- concentration of groundwater at the LS site (1.4 ± 0.8 µM) was around detection limit and is similar to porewater (Figure 6).

Porewater

The average NH_4^+ concentration of porewater at the RP site is 320.9 ± 190.2 µM and much higher than the NH_4^+ concentration of groundwater (0.6 ± 1.0 µM) (Figure 5). On the other hand, the NO_3^- concentration of porewater (0.4 ± 0.1 µM) is much lower than the NO_3^- concentration of groundwater (29.9 ± 7.6 µM) (Figure 6). This is potentially due to the existence of dissimilatory NO_3^- reduction to NH_4^+ (DNRA). DNRA is a biological process that reduces NO_3^- to NH_4^+. DNRA has been reported to be the dominant NO_3^- process in the sediments of Baffin Bay due to the existence of S^{2-}, which facilitates DNRA but may inhibit other processes like denitrification (An and Gardner, 2002). The porewater NO_3^- is almost all converted to NH_4^+, so the fractionation of DNRA should not be significant and the generated $\delta^{15}N\text{-}NH_4^+$ from DNRA would be similar to the $\delta^{15}N\text{-}NO_3^-$ of groundwater (+22.1 ± 6.1‰) (Figure 9). But the $\delta^{15}N\text{-}NH_4^+$ of porewater (+9.2 ± 3.4‰) is lower than the $\delta^{15}N\text{-}NO_3^-$ of groundwater (Figure 8).

This is likely due to the likely occurrence of mineralization of organic nitrogen in porewater. The sediment is a sink of particulate organic nitrogen (PON) (e.g., algae). The nitrogen isotopic composition of algae is about +7.5 ± 2.2‰ (Doi et al., 2010). The fractionation due mineralization causes $\delta^{15}N\text{-}NH_4^+$ values lower than +7.5 ± 2.2‰, which when mixed with the enriched $\delta^{15}N\text{-}NH_4^+$ from DNRA, leads to $\delta^{15}N\text{-}NH_4^+$ of porewater around +9.2 ± 3.4‰. The DON concentration of porewater (38.3 ± 15.8 µM) is higher than the DON of groundwater (28.3 ± 14.0 µM) (Figure 7). This is because PON buried in the sediment can be broken down into smaller molecules by bacteria and dissolve in porewater, explaining the increased DON concentration. The $\delta^{15}N$-PON has been reported to be +7.5 ± 2.2‰, (Doi et al., 2010) and this biological braking down process of PON may generate even lower $\delta^{15}N$-DON, which when mixed with the enriched $\delta^{15}N$-DON of groundwater (+24.4 ± 3.3‰), results in a $\delta^{15}N$-DON value of porewater of +15.5 ± 2.5‰ (Figure 11).

Similarly, at LS, due to breaking down" of PON and mineralization, porewater contains a high concentration of NH_4^+ (243.4 ± 118.0 µM) and DON (34.1 ± 15.9 µM) but depleted NO_3^- (0.8 ± 0.7 µM) (Figure 5-7). However, the area around LS is undeveloped, and the sampling sites are frequently flooded when compared to the more developed/residential area around RP. RP is influenced by enriched $\delta^{15}N$-DON from septic, which percolates to water table, thus the source of relatively enriched $\delta^{15}N\text{-}NH_4^+$ of porewater at RP site. The enriched $\delta^{15}N\text{-}NH_4^+$ source is not evident in porewater at LS as there is not an expected nearby source of septic. Thus, this explainsthe decreased concentration and isotopic composition of NH_4^+ (243.4 ± 118.0 µM and +8.0 ± 5.2‰, respectively) and DON (34.1 ± 15.9 µM and +14.0 ± 3.5‰, respectively) of porewater compared with RP (Figure 5-7 and11).

Surface water

The nitrogen pool in surface water is dominated by DON (59.0 ± 11.4 µM) (Figure 7), which constitutes 98% of the nitrogen pool at both LS and RP. Porewater can be a source of DON to surface water. However, δ^{15}N-DON values of surface water (+12.5 ± 1.0‰ at RP and +12.5 ± 1.6‰ at LS) are lower than porewater (Figure 11). This suggests an additional source of DON other than porewater. As DON is released to the surface, it will be consumed by the phytoplankton, which prefers to use light nitrogen (Kendall et al., 2007). This process should have increased the δ^{15}N-DON of surface water. However, other sources (e.g., fertilizer, livestock waste and atmospheric deposition) with depleted δ^{15}N-DON signatures contribute to the DON pool of surface as well (Felix and Campbell, 2019), explaining the lower δ^{15}N-DON. Similarly, porewater is a source of NH_4^+. But NH_4^+ can be quickly assimilated by microorganism as it is reaching the surface. Hence, NH_4^+ concentration is depleted at both RP (0.6 ± 1.0 µM) and LS site (0.6 ± 1.3 µM) (Figure 6). Porewater is not a significant NO_3^- source, and NO_3^- coming from other sources is limited due to the limited precipitation and riverine input to the bay (Felix et al., 2021). Additionally, NO_3^- that reaches surface water can be quickly processed. Therefore, NO_3^- was also depleted in surface water (0.4 ± 0.4 µM at RP site and 0.7 ± 0.9 µM at LS site) (Figure 6).

Surface water DIN and DON seasonal variation

Seasonal variation of DIN concentrations and isotopic composition in the bay surface waters

Generally, concentrations of NH_4^+ were around detection limit and the highest concentration was measured at RP-S1 (4.1 ± 5.8 µM), RP-S2 (0.6 ± 0.9 µM) and LS-S1 (4.0 ± 5.7 µM) in spring and at LS-S2 (0.6 ± 0.9 µM) in summer (Figure 5). This is potentially due to the increased rate of photoproduction that produces DIN (e.g., NH_4^+) from DON (Vähätalo and

Järvinen, 2007). This process is stimulated by solar radiation expected in spring and summer, raising NH_4^+ concentrations. Also, spring and summer were the only two seasons with NH_4^+ concentrations high enough for isotope analysis. The lowest $\delta^{15}N\text{-}NH_4^+$ at RP-S1 is observed in spring (+5.2 ± 2.9‰) (Figure 8). The only available $\delta^{15}N\text{-}NH_4^+$ values for RP-S2 (+7.9‰) and LS-S1(+2.1‰) were for samples collected in spring.

Similarly, NO_3^- concentrations fluctuate around the detection limit. The highest NO_3^- concentrations at RP-S1 (1.5 ± 1.4 µM), LS-S1 (1.5 ± 1.4 µM) and LS-S2 (2.7 ± 1.2 µM) were observed in winter (Figure 6). At RP-S2, NO_3^- does not show significant seasonal variation and the highest concentration (0.4 ± 0.2 µM) was observed in fall. The only available $\delta^{15}N\text{-}NO_3^-$ value (+26.1‰) is observed at RP-S1 in winter (Figure 9). This enriched $\delta^{15}N\text{-}NO_3^-$ may indicate that nitrification of NH_4^+ was the source of NO_3^- as the fractionation of nitrification is reported to be significant (+26‰) (Granger and Wankel, 2016). However, due to the lack of data points, this hypothesis cannot be verified right now.

Seasonal variation of DON concentrations and isotopic composition in the bay surface waters

The highest and lowest DON concentrations were observed in summer (76.1 ± 5.3 µM) and winter (46.4 ± 3.1 µM), respectively, in all surface water transects, except for LS-S2 (Figure 9). This is associated with nutrient input. The DON pool in surface water is fueled by heavy rainfall and runoff during summer while the DON input from rainfall, runoff and SGD decrease in winter (Sorooshian et al., 2014) (Figures 3 and 21). LS-S2 showed a slightly higher DON concentration in winter but no significant seasonal variation was observed. RP-S2 showed the highest $\delta^{15}N\text{-DON}$ in summer (+14.2 ± 0.4‰) (Figure 11). This is due to the enriched solar radiation during summer, which enables photoproduction of DIN from DON. Photoproduction preferentially uses the lighter ^{14}N, leaving the residual DON enriched in $\delta^{15}N$ during summer.

However, the study area is located in a subtropical zone, where it can receive up to 5,000 Wh/m^2 of global horizontal solar radiation in September or October (NREL, 2007). So photoproduction continues to be active during fall. Continued photochemical processing of DON throughout summer and into fall may explain why the highest δ^{15}N-DON occurred in fall at both RP-S1 (+12.3 ± 1.8‰) and LS-S1 (+12.0 ± 2.3‰). LS-S2 (+11.8 ± 3.0‰) showed the highest δ^{15}N-DON in winter. This is expected due to the decreased rainfall and runoff in winter (Figure 3). Winter is the driest season of the year that receives the lowest precipitation in study area (Sorooshian et al., 2014) leading to a decreased DON contribution from fertilizer, livestock waste and atmospheric deposition, which delivers DON to the surface of the bay through rainfall or runoff. Fertilizer (-0.6 ± 0.3‰), livestock waste (+3.9 ± 0.4‰) and atmospheric deposition (+4.4 ± 0.3‰) contain depleted δ^{15}N-DON (Felix and Campbell, 2019). LS-S2 may have a high DON contribution from sewage (+14.1‰) or septic (+20.0 ± 6.8‰) that is enriched in δ^{15}N resulting in the highest δ^{15}N-DON in winter (Felix and Campbell, 2019; Felix et al., 2021). However, the DON flux through SGD remained low in winter (Figure 21). Hence sewage is believed to be the dominant DON source at LS-S2 in winter potentially associated with more use of winter vacation homes and increasing output to the wastewater treatment plants.

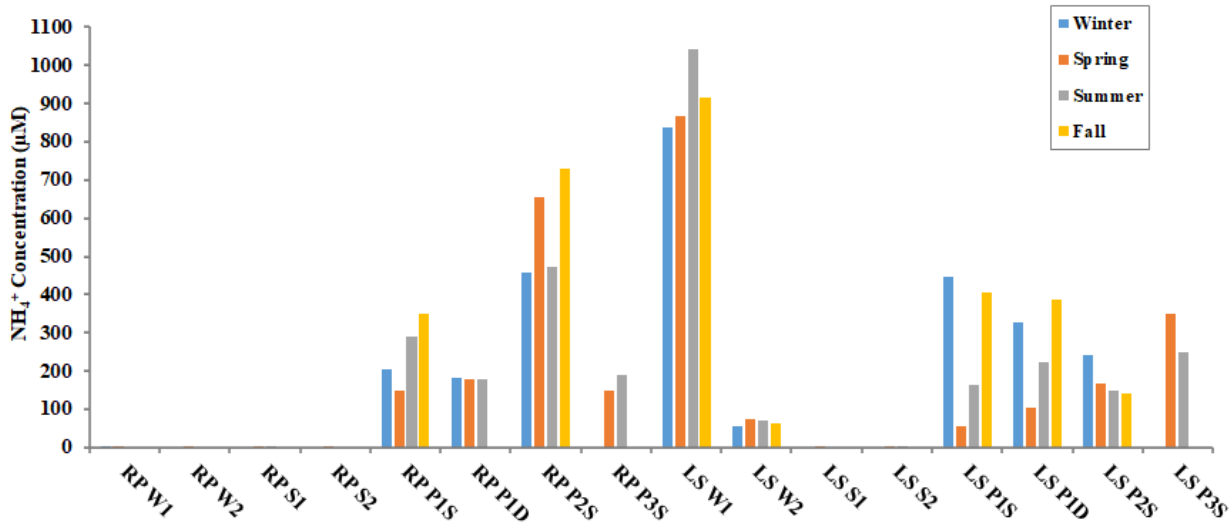

Figure 5. NH4+ variation at both RP and LS transects.

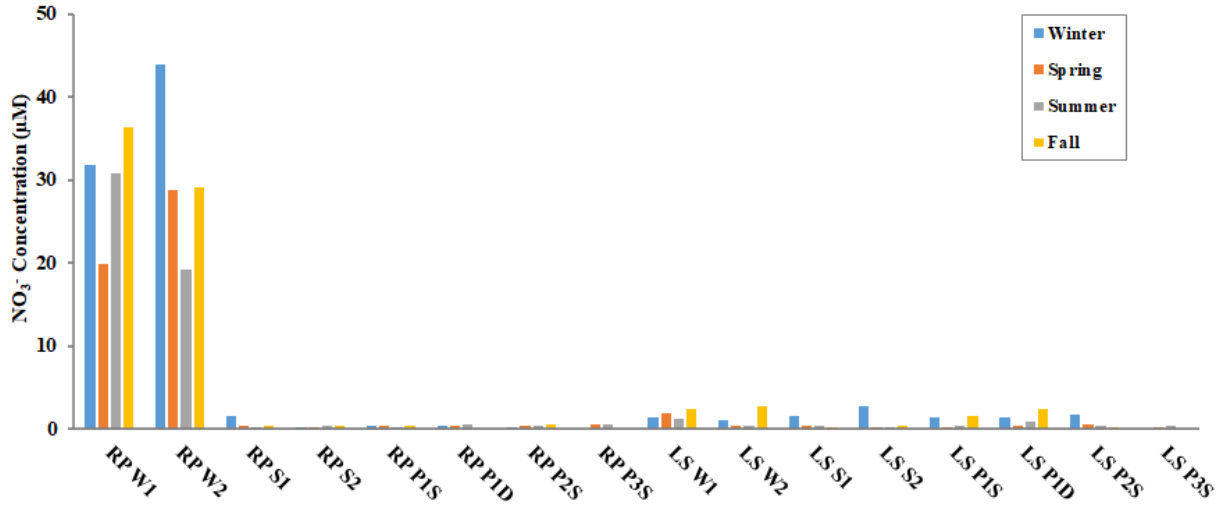

Figure 6. NO_3^- variation at both RP and LS transects. Most of the NO2- concentration in this study is lower than 2% of NO_3^- + NO_2^- and is not significant. So NO_2^- is not reported.

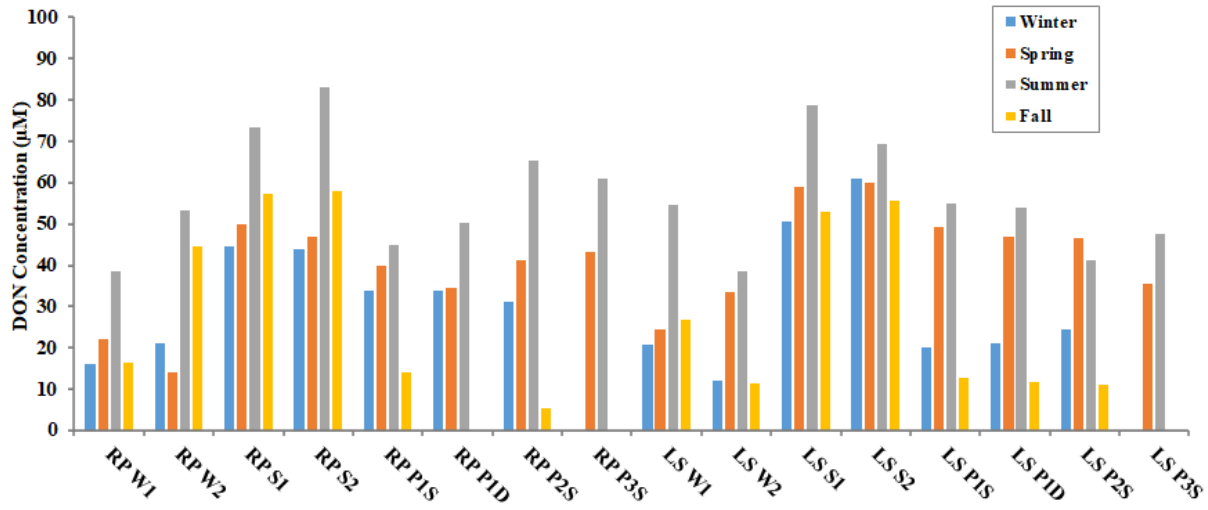

Figure 7. DON variation at both RP and LS transects.

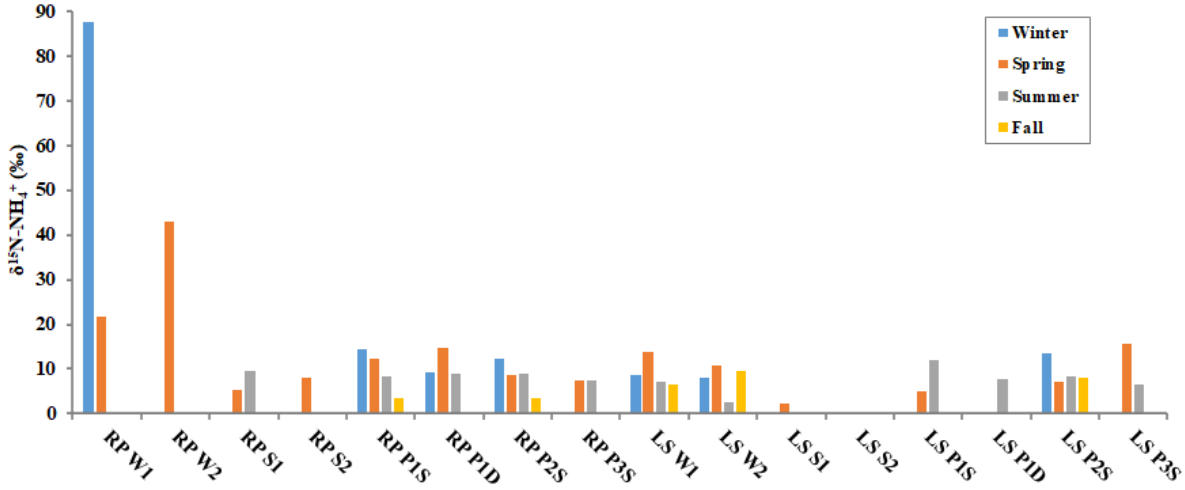

Figure 8. $\delta^{15}N\text{-}NH_4^+$ variation at both RP and LS transects.

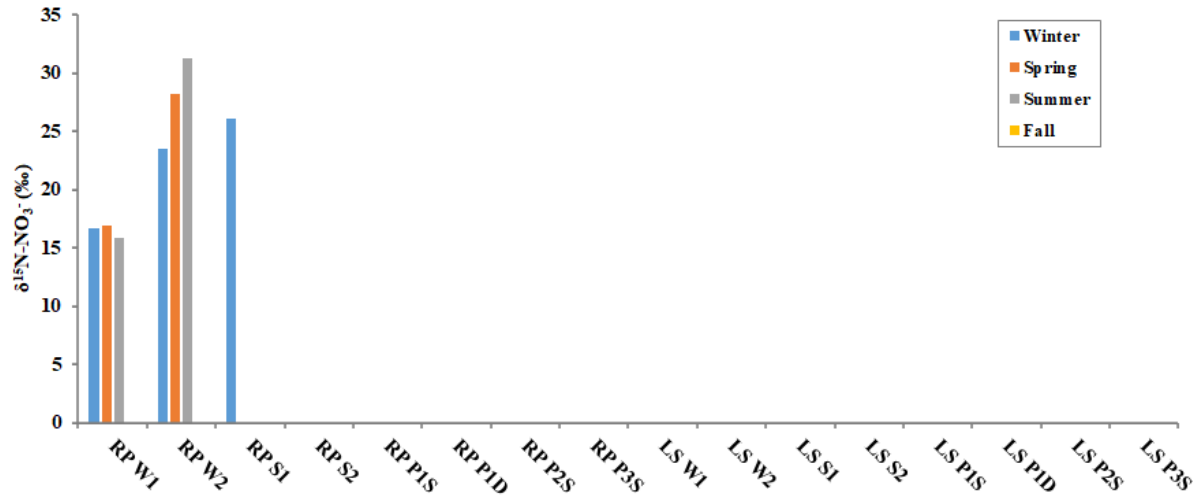

Figure 9. $\delta^{15}N\text{-}NO_3^-$ variation at both RP and LS transects.

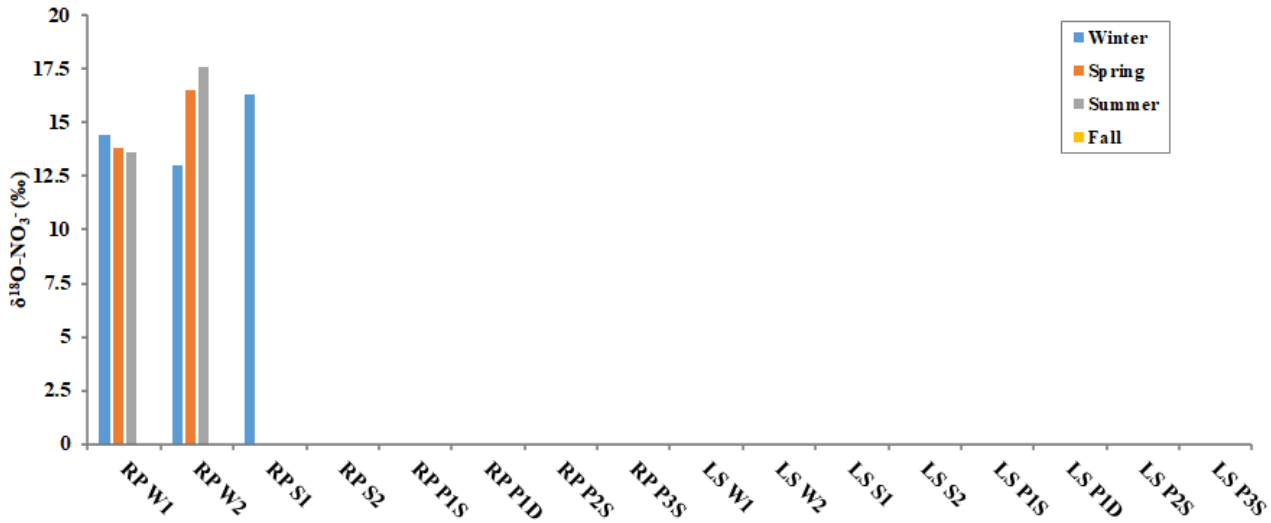

Figure 10. $\delta^{18}O\text{-}NO_3^-$ variation at both RP and LS transects.

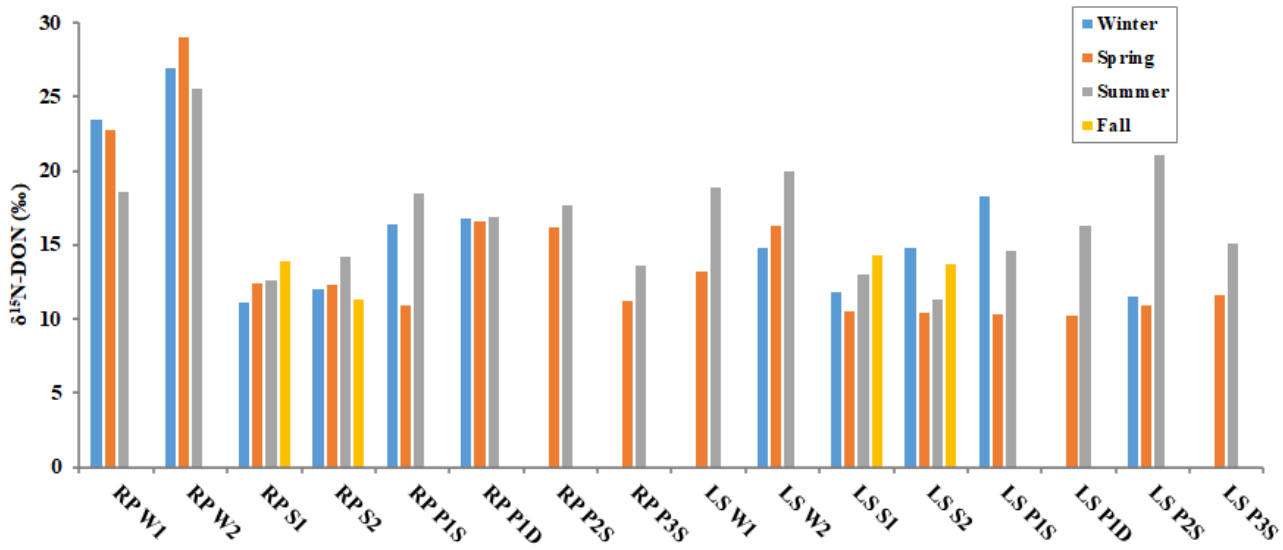

Figure 11. δ^{15}N-DON variation at both RP and LS transects.

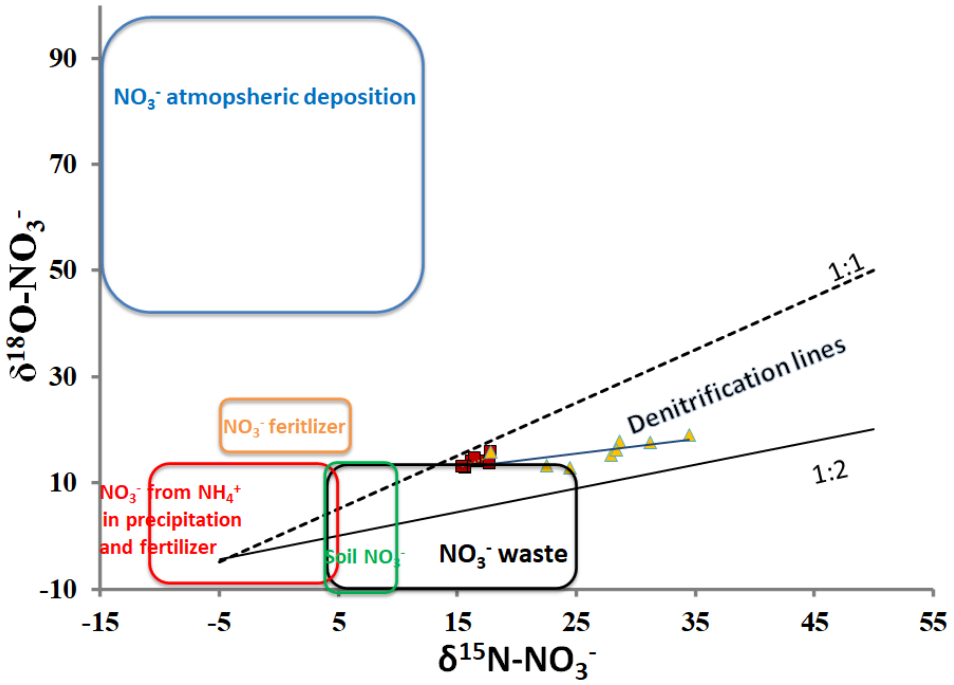

Figure 12. Dual nitrate isotope Kendall source plot. Red squares indicate RP-W1 samples and yellow triangles indicate RP-W2 samples.

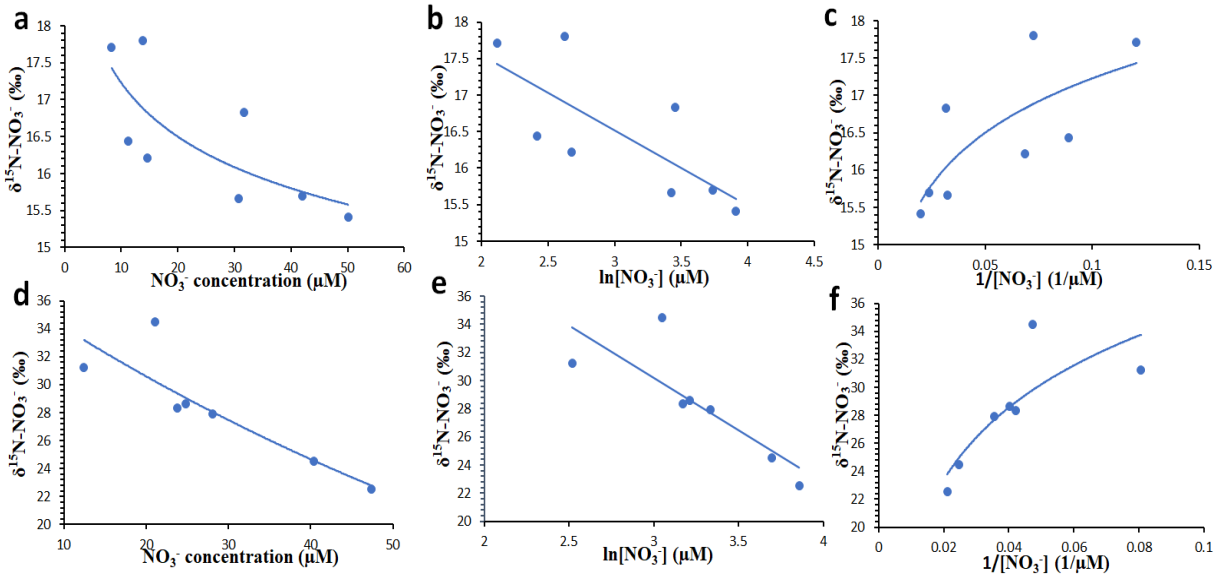

Figure 13. Figure 12. Keeling plots. a-c are plots of δ^{15}N-NO_3^- versus the NO_3^- concentration, inverse NO_3^- concentration and natural logarithm of the concentration, respectively, at RP-W1. d-f are plots of δ^{15}N-NO_3^- versus the NO_3^- concentration, inverse NO_3^- concentration and natural logarithm of the concentration, respectively, at RP-W2. When δ^{15}N-NO_3^- plots against the concentration of NO_3^-, a steep curve means mixing is the dominant process. When δ^{15}N-NO_3^- plots against the inverse NO_3^- concentration, a curve also means mixing is the dominant process. When δ^{15}N-NO_3^- plots against the natural logarithm of NO_3^- concentration, a curve means mixing is a minor process. The mild curves in both Figure 13a and 13d, the straight line in both Figure 13b and 13e, and the curves in both Figure 13c and 13f all indicate that mixing is an insignificant process at RP-W1 and RP-W2.

Isotope mixing model (DON source contributions)

Results from the isotope mixing model indicate that sewage or septic effluent is the dominant DON source to Baffin Bay whether near a septic system/residential dominated area (RP site) or near an underdeveloped, more agricultural dominated area (LS site) (Figure 14, 15). The high sewage/septic influence can be attributed to septic effluent discharge to groundwater and/or wastewater discharge but high DON concentrations and enriched δ^{15}N-DON in the groundwater may indicate the former. The sewage/septic contribution at RP-S1 (46.5 ± 4.9%), RP-S2 (45.9 ± 5.3%), LS-S1 (45.9 ± 6.9%) and LS-S2 (46.5 ± 8.6%) site shows no signification

spatial variation. The highest sewage/septic contribution at RP-S1, RP-S2 and LS-S1 is observed in fall, summer and fall, respectively. DON from either sewage or septic is enriched in $\delta^{15}N$ and the high $\delta^{15}N$-DON at RP-S1, RP-S2 and LS-S1, respectively, in fall, summer and fall indicates increased septic/sewage input (Figure 11). Both LS-S1 and LS-S2 exhibit the least sewage/septic contribution (37.6% and 37.4%, respectively) but highest fertilizer (18.2% and 18.2%, respectively), livestock waste (21.8% and 21.6%, respectively) and atmospheric deposition (22.5% and 22.8%, respectively) contribution in spring (Figure 15). This is due to the increased rainfall in spring (Figure 3). The study area received 101.7-152.4 mm of precipitation in May 2020 (Sorooshian et al., 2014). The increased rainfall not only increases the DON input from atmospheric deposition, but also increases DON input from fertilizer and livestock waste via surface or subsurface runoff. April/May in the area is also a time of first fertilizer application of the year.

RP-S1 and PR-S2 received the least contribution of sewage/septic (40.4% and 41.3%, respectively) but highest contribution of fertilizer (17.3% and 17.4%, respectively), livestock waste (20.7% and 20.7%, respectively) and atmospheric deposition (21.7% and 20.6%, respectively) in winter and fall, respectively (Figure 14). The study area received 76.3-101.6 mm of precipitation in September 2020. The increased rainfall not only increases the DON input from atmospheric deposition, but also increases DON input from fertilizer and livestock waste. The residue of fertilizer and livestock waste can be delivered to watersheds and further into the bay through runoff after rain events, which explains the high DON input of fertilizer, livestock waste and atmospheric deposition in fall at RP-S2. However, winter in the study area received the least precipitation but showed the highest DON contribution of fertilizer, livestock waste and atmospheric deposition. This is likely related to the DON flux via SGD. The DON flux through

SGD remained low during winter at RP (Figure 21), reducing the contribution of sewage/septic and in turn increase the relative contribution of fertilizer, livestock waste and atmospheric deposition. The average concentration and isotope composition of DON and DIN along the transects at the RP and LS sites are summarized in Figure 16 and 17, respectively.

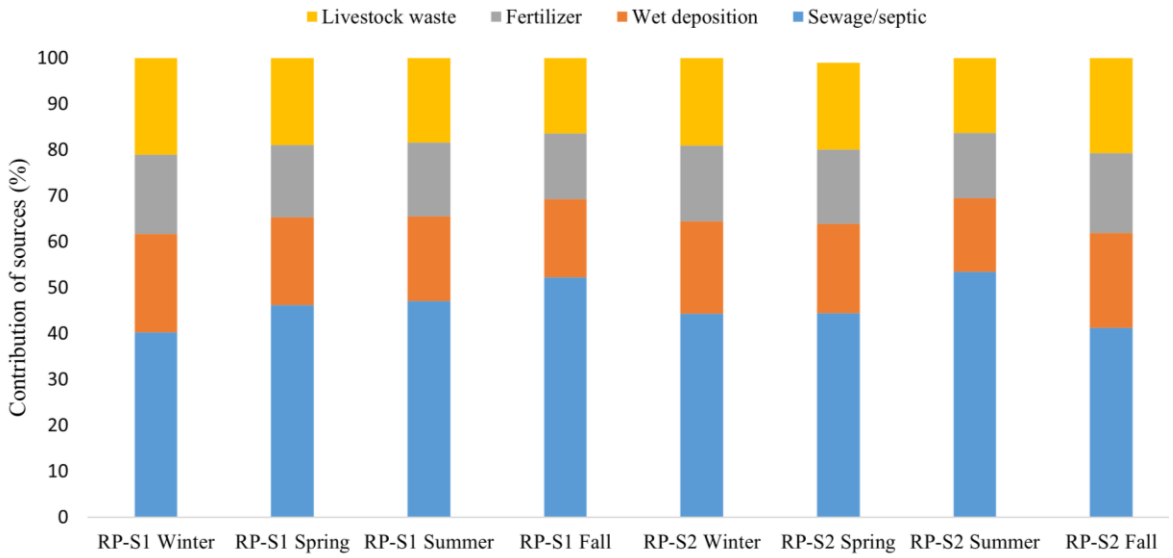

Figure 14. DON source apportionment at RP site.

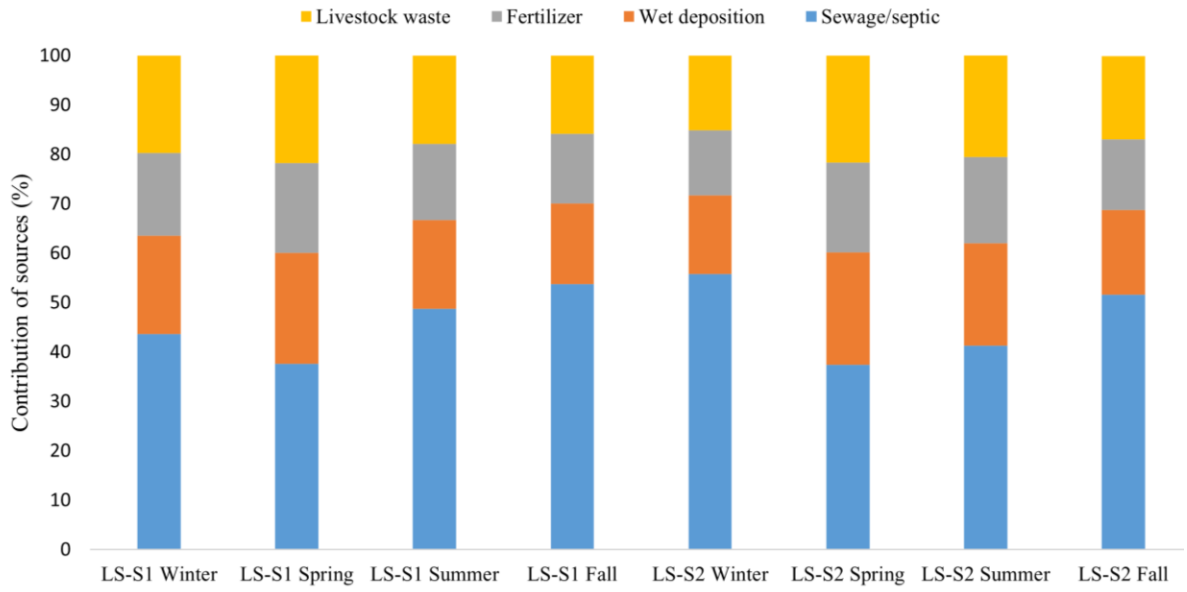

Figure 15. DON source apportionment at LS site.

Processing of DON and DIN along the land - water transects

The average concentration and isotope composition of DON and DIN along the transects at the RP and LS sites are summarized in Figure 16 and 17, respectively. The RP site is dominated by the soil type of sand, which can lead to nitrogen contamination from septic system to water table (Felix et al., 2021; Qiu et al., Unpublished work). Septic effluent consists of a large portion of NH_4^+ (70 to 90%) but only a small portion of NO_2^-/NO_3^- (~ 0.4%) due to its anaerobic condition (Harrison et al., 2000; Lusk et al., 2017). As septic effluent percolates through the soil, NH_4^+ is depleted and converted to NO_3^- due to nitrification. Denitrification rate in the soil type of sand is minor so NO_3^- reaches the water table before being completely processed. This is indicated by the noticeable NO_3^- concentration at RP-W1 (29.7 ± 7.0 µM) and RP-W2 (30.2 ± 10.2 µM) while insignificant NH_4^+ concentration (1.0 ± 1.3 µM at RP-W1 and 0.2 ± 0.3 µM at RP-W2). The DON can be consumed as septic effluent percolates the soil depth. But this process is not significant as DON only favors certain types of microorganism, leading to

23.3 ± 9.1 µM and 33.3 ± 16.2 µM of DON at RP-W1 and RP-W2, respectively. The groundwater flows into porewater and releases nutrients like DON to the surface through SGD. However, the NO_3^- from groundwater is depleted and converted to NH_4^+ through DNRA as it reaches porewater (0.4 ± 0.1 µM). Including DNRA, the mineralization of organic nitrogen is another NH_4^+ source and generates depleted δ^{15}N-NH_4^+ in the sediment, lowering δ^{15}N-NH_4^+ at porewater (+9.2 ± 3.4‰). The DON from groundwater is mixed with DON generated from "broken down" PON, leading to an increased DON concentration at porewater (38.3 ± 15.8 µM). As δ^{15}N-PON (+7.5 ± 2.2‰) is much lower than the δ^{15}N-DON of groundwater (+24.4 ± 3.3‰), even though this "broken down" process generates slightly enriched δ^{15}N-DON, the δ^{15}N-DON of porewater (+15.5 ± 2.5‰) is reduced compared with groundwater. Although NO_3^- was depleted, NH_4^+ and DON continue to be released to the bay surface water. As NH_4^+ is reaching the surface it is quickly processed and assimilated by microorganisms, leading to a depleted NH_4^+ concentration at surface water (1.3 ± 1.7 µM at RP-S1 and 0.2 ± 0.3 µM at RP-S2). DON is also consumed by phytoplankton, which would have increased the δ^{15}N-DON of surface water. Nevertheless, other sources (e.g., fertilizer, livestock waste and atmospheric deposition) with depleted δ^{15}N-DON contribute DON to the surface water (Felix and Campbell, 2019) and lower the δ^{15}N-DON of surface water (+12.5 ± 1.0‰ at RP-S1 and +12.5 ± 1.1‰ at RP-S2). Those other sources contribute limited NO_3^- to the surface of the bay and NO_3^- is quickly processed as it reaches the surface water. As a result, the DON in surface water (56.2 ± 10.9 µM at RP-S1 and 58.0 ± 15.5 µM at RP-S2) constitutes 97.9% of the nitrogen pool.

The LS site is dominated by the soil type of salt flat and is frequently flooded. This explains why the groundwater at LS site contains high NH_4^+ concentration (914.2 ± 78.8 µM at LS-W1 and 64.6 ± 6.1 µM at LS-W2) (Figure 17). The NH_4^+ concentration at LS-W1 is even

higher than porewater (243.4 ± 118.0 µM). This is due to the further mineralization of organic nitrogen as porewater intrudes groundwater, leaving an increased δ^{15}N-DON (+16.1 ± 2.9‰ at LS-W1 and +17.0 ± 2.2‰ at LS-W2) but decreased DON concentration (31.7 ± 13.5 µM at LS-W1 and 23.9 ± 12.3 µM at LS-W2) at groundwater compared with porewater. The NH_4^+ concentration at LS-W2 is much lower. This is because that LS-W2 is farther away from the bay and is less affected by the porewater. Also, NH_4^+ can be quickly processed as it travels through the water table, leading to a reduced concentration at LS-W2. The NO_3^- concentration of groundwater at LS is around detection limit (1.7 ± 0.4 µM at LS-W1 and 1.1 ± 1.0 µM at LS-W2) as the groundwater is heavily influenced by porewater where the NO_3^- is limited (0.8 ± 0.7 µM). Porewater also contains high concentration of NH_4^+, which is predominantly produced from the mineralization of organic nitrogen. The fractionation of mineralization is small (-1.43‰ to -2.3‰) and δ^{15}N-PON is around +7.5 ± 2.2‰ (Doi et al., 2010; Möbius, 2013), resulting in δ^{15}N-NH_4^+ being around +8.0 ± 5.2‰ in porewater. The mineralization of PON also generates DON with slightly enriched δ^{15}N, leading porewater DON to have concentrations of 34.1 ± 15.9 µM and δ^{15}N-DON values of +14.0 ± 3.5‰. Like the RP site, NH_4^+ and DON continue to be released to the surface of the bay at LS site. NH_4^+ is quickly processed and assimilated by microorganism, leading to a depleted NH_4^+ concentration at surface water (1.0 ± 1.7 µM at LS-S1 and 0.2 ± 0.2 µM at LS-S2). Similarly, mixing with δ^{15}N-DON depleted sources at the LS site makes δ^{15}N-DON of surface water +12.4 ± 1.4‰ at LS-S1 and +12.6 ± 1.8‰ at LS-S2. NO_3^- concentration at the LS site remains around detection limit (0.6 ± 0.5 µM at LS-S1 and 0.9 ± 1.1 µM at LS-S2). Here the DON in surface water (60.3 ± 11.0 µM at LS-S1 and 61.4 ± 4.9 µM at LS-S2) constitutes about 97.8% of nitrogen pool.

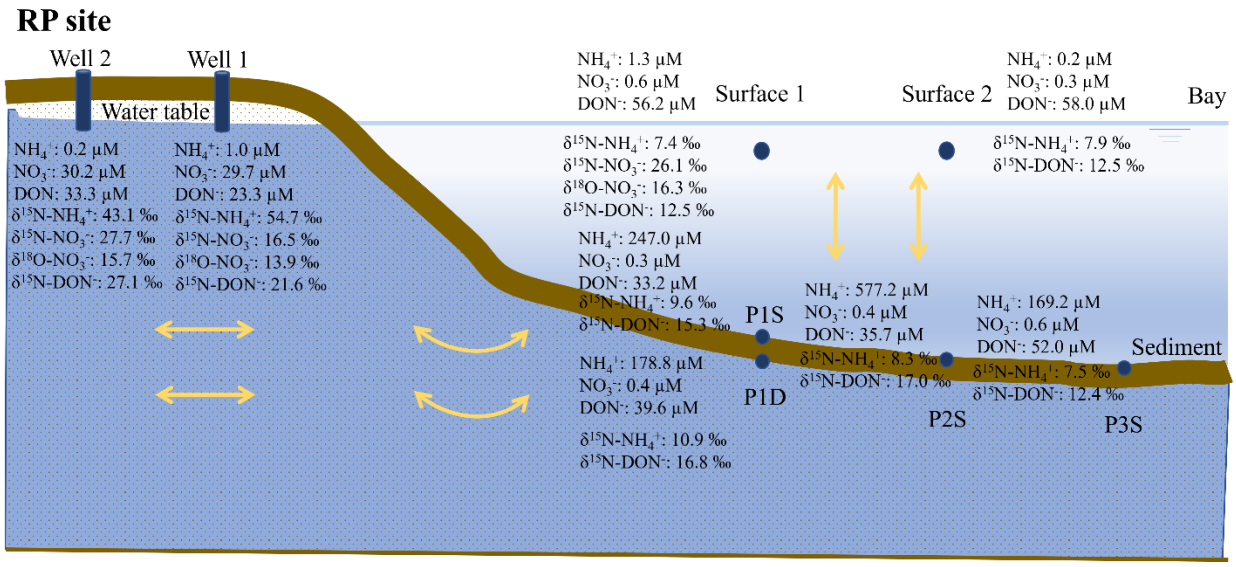

Figure 16. The concentration and isotope composition of DON and DIN at RP site.

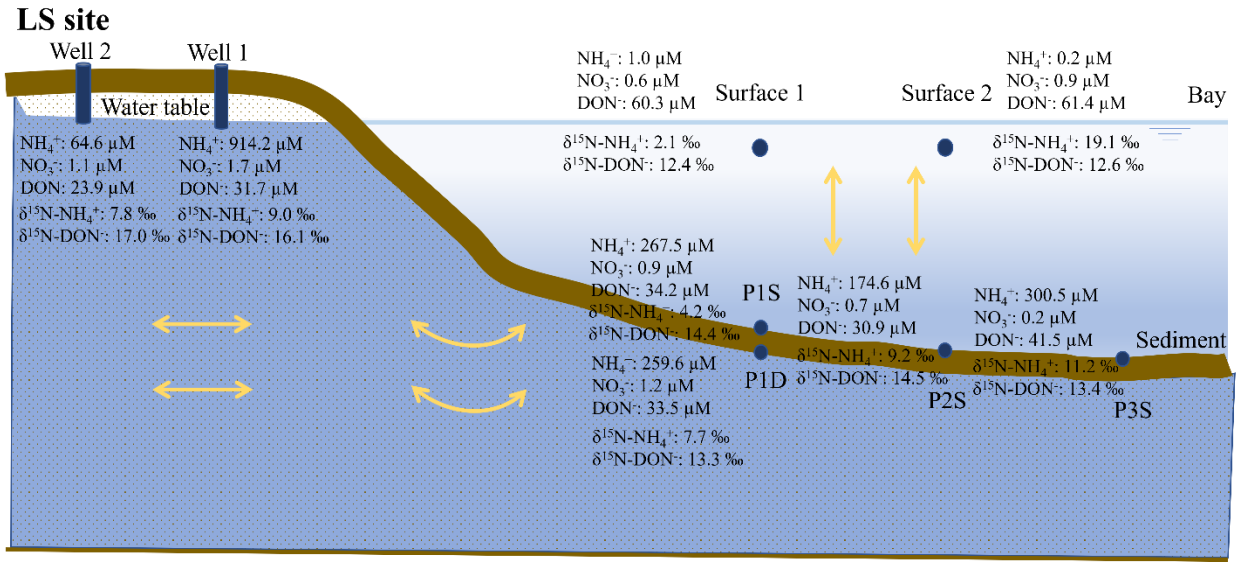

Figure 17. The concentration and isotope composition of DON and DIN at LS site

Submarine Groundwater Discharge

Darcy Groundwater Discharge Rate Estimates

Darcy's groundwater estimates are expected to represent the fresh terrestrial input. In this study because monitoring wells are very close to the coastline, the discharge derived from Darcy's law are not only influenced by terrestrial hydraulic gradients, but tidal pumping (Figure 18).

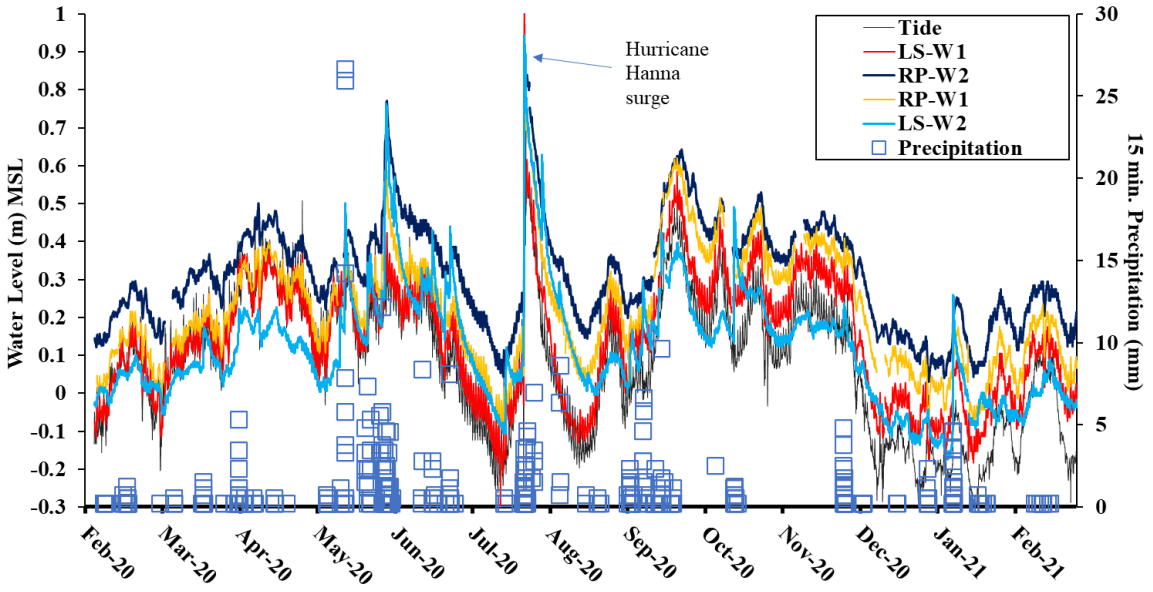

Figure 18. Groundwater level at both LS and RP measured with an In-Situ data logger in each of the four wells. Tidal data is from (NOAA, 2020) Monthly precipitation at RP and LS from (NOAA/CO-OPS, 2021). Hurricane Hanna made landfall July 25th, 2020.

The only representative terrestrial fresh component is well 2 at the RP which had salinities varying between 5 and 9 (average 12) for the monitoring period, compared to the nearshore well 1 with salinities from 48 to 88 (average 61). Both wells at LS had salinities above seawater ranging from 65 and 82 (average 72), for well 1 (nearshore) and 51 and 63 (average 55) for the further inland well 2. However, both more inland wells (well 2 at RP and LS) are least influenced by tides, thus are selected to represent the terrestrial input, although not fresh. Using an effective porosity of 0.05 for the Chicot Aquifer (Young, 2016) was applied to Darcy estimates to convert from specific discharge to groundwater velocity (v). The terrestrial groundwater seepage velocities (or groundwater discharge rates) ranged from –10 to 32.4 $cm \cdot d^{-1}$ and averaged 8 $cm \cdot d^{-1}$ for the one year of monitoring. The lowest seepage rates were measured in April-May and September-October (Figure 19).

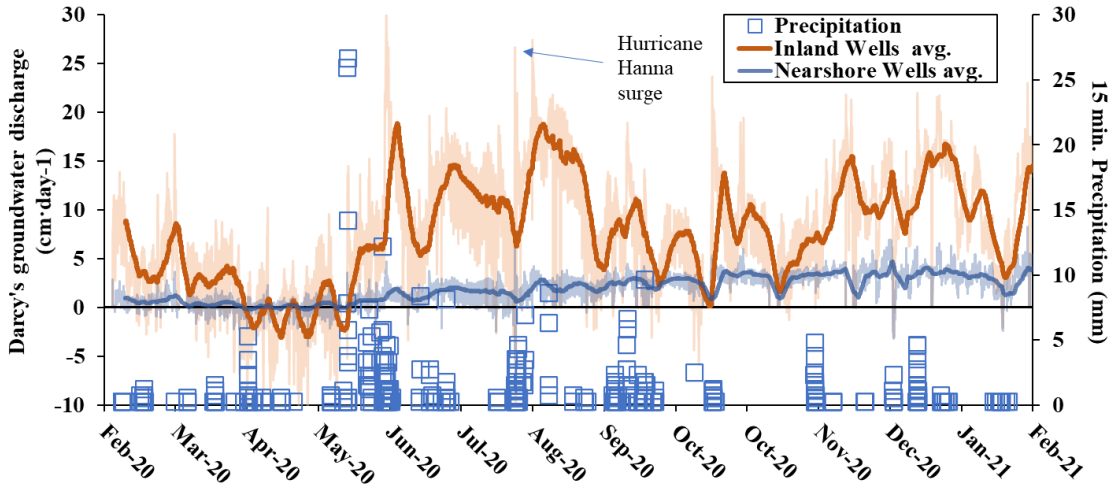

Figure 19. Darcy seepage velocity (or groundwater discharge rates) for inland wells (LS and RP well 2) and nearshore wells (LS and RP well 1). Monthly precipitation in the area (NOAA/CO-OPS, 2021).

Seepage velocities determined from the nearshore wells are essentially the recirculated saline component as a result of tidal influences. These rates ranged between -3 to 5 $cm \cdot d^{-1}$ with the lowest rates during the April-May interval. A negative flux using Darcy's law indicates that seawater is intruding the aquifer. Although some fluctuations exist, there are least significant when compared to the terrestrial inputs and the most significant changes seem to correspond among the two environments (Figure 19).

^{222}Rn-derived SGD Estimates

Porewater ^{222}Rn, collected from two depths at two locations at each site, ranged from 4.8 to 4,001 $Bq \cdot m^3$ ($\bar{x}$: 398.2 $Bq \cdot m^3$, n=60). The activities exhibit some seasonal trends with the average decreasing from February 2020 to May 2020 (winter 2019 to spring 2020) and increasing from June 2020 to August 2020 (summer 2020), followed by a decline from September 2020 to January 2021 (fall 2020 and winter 2021). Groundwater ^{222}Rn ranged from 82.9 to 50,734 $Bq \cdot m^3$ ($\bar{x}$: 7,772 $Bq \cdot m^3$ n=40) and follows a similar seasonal pattern as porewater.

Groundwater ^{222}Rn activities were observed to increase in summer 2020, and decrease in fall 2020 and winter 2021. The exception is the increasing ^{222}Rn activities from March to May 2020 (spring 2020). Surface water ^{222}Rn did not follow the same trends as the groundwater (porewater and well water), surface water ^{222}Rn decreased during summer 2020 (from June to August) and increased in fall 2020 (September to November 2020).

SGD calculations using the average ^{222}Rn activities in the four monitoring wells ranged from 2.9 to 40.4 cm·d^{-1} ($\bar{x}$: 16.7 cm·d^{-1}, n=21). The highest average rate over the course of the study of 18.2 cm·d^{-1} (n=11) was measured at Site 55 (or LS). The average SGD rate at Riviera Fishing Pier site was 15.1 cm·d^{-1} (n=10). At both locations monthly SGD rates follow a similar trend, except for February to March 2020, when for SGD is decreasing at Site 55 while increasing at Riviera Fishing Pier. During spring (March to May 2020) and fall (September-October) both locations show a decrease in SGD (Figure 20), which is similar to Darcy's SGD trends. In late fall and winter SGD increased at both locations.

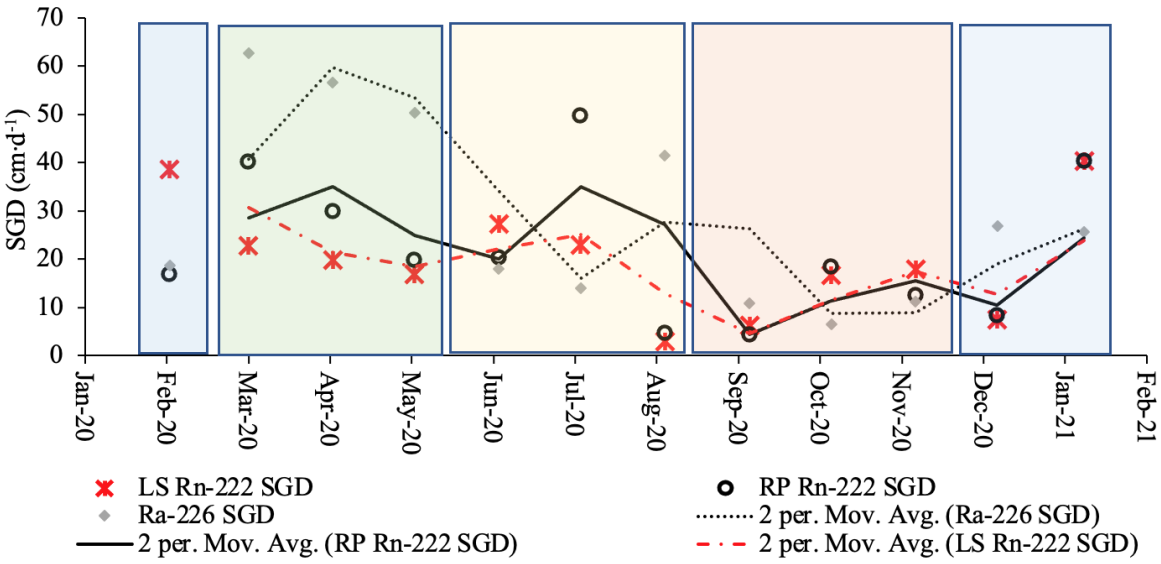

Figure 20. Site specific radon-derived SGD rates and overall radium-derived SGD rates. Vertical colored panels represent seasons (blue – winter includes December, January, and February; green – spring includes March, April, and May; yellow – summer includes June, July, and August; and orange – fall, includes September, October, and November).

Using the ^{222}Rn activities of deeper wells located in the Baffin Bay (e.g., watershed well end member), which is a constant throughout the study period (7,805 $Bq \cdot m^3$), SGD rates over the course of the study show an overall decreasing trend.

^{226}Ra -derived SGD Estimates

Radium-derived SGD calculations represent the older groundwater inputs, usually of saline make up. Higher ^{226}Ra SGD rates could be associated with inputs of more radium enriched groundwater, which is generally from deeper and more regional flowpaths. In this study, the average ^{226}Ra activities in the four monitoring wells were used as the endmember, and given the shallow and tidal influence (i.e., seawater recirculation that is likely more depleted in radium), the resulting SGD rates may be overestimated. In addition, the rates produced from ^{226}Ra in this study, are integrated over the Laguna Salada, thus, they are an average of the bay.

Overall SGD rates in Laguna Salada ranged from 7 to 63 $cm \cdot d^{-1}$ ($\overline{x}$: 26 $cm \cdot d^{-1}$, n=21). The highest rate over the course of the study was measured in March. Rates from ^{222}Rn (also referred as total SGD rates, including saline and fresh inputs) were also elevated in March, but were slightly lower than the maximum of 40 $cm \cdot d^{-1}$ in December (Figure 20). The minimum rate was measured in October, with more than double corresponding average total SGD rates. Similar to radon-derived rates, there is an overall decreasing trend in SGD from spring ($\overline{x}$: 57 $cm \cdot d^{-1}$), summer ($\overline{x}$: 25 $cm \cdot d^{-1}$) to fall ($\overline{x}$: 10 $cm \cdot d^{-1}$), with an increase in winter ($\overline{x}$: 24 $cm \cdot d^{-1}$).

Nutrient Flux Rates

Nutrient fluxes (in $\mu mol\ m^{-2} \cdot d^{-1}$) were calculated as the product of local groundwater and porewater average nutrient concentrations and radon-derived SGD rates using the average groundwater endmember. Since porewater samples were collected at different range depths, we

include nutrient fluxes derived from the average nutrient concentrations of shallow and deep porewater depths.

The largest NO_3^-+ NO_2^- (referred as NO_x going further) flux was derived using the average well concentrations, referred to us terrestrial. That is because groundwater was always about two orders of magnitude higher than porewaters. Terrestrial NO_x fluxes were the highest at LS in February 2021 (25,614 μmol·d^{-1}) and January 2020 (25,614 μmol·d^{-1}) while the lowest transpired in August (Figure 21a). Fluxes decreased from February to June 2020, with an increase in July, similar to March. After dipping in August, the NO_x fluxes increased and fluctuated until January 2021, the highest calculated flux. The deeper porewater (~1m) endmember concentrations resulted in NO_x fluxes about one order of magnitude lower than the terrestrial ones, likely due to transformation of NO_3^- to reduced forms like NH_4^+ along the transport path of groundwater within the anoxic, hypersaline subterranean estuary. Shallow porewater fluxes were slightly lower than those from deeper porewater, but both showed a similar pattern with increasing magnitudes beginning in September.

Similar to NOx, the largest NH_4^+ flux was derived using the average well concentrations, but when compared to those derived from porewaters, they were similar in range, except for January 2021 and February 2020. For these two months, both groundwater and deep porewater derived fluxes are higher at LS (Figure 21b, b'. b"). At both locations, LS and RP, the terrestrial NH_4^+ fluxes exceeded those from porewater until June. Beginning with July, the fluxes associated with shallow porewater were slightly higher, which indicates production of NH_4^+ in sediments from sources other than groundwater (see section on nutrients and sourcing).

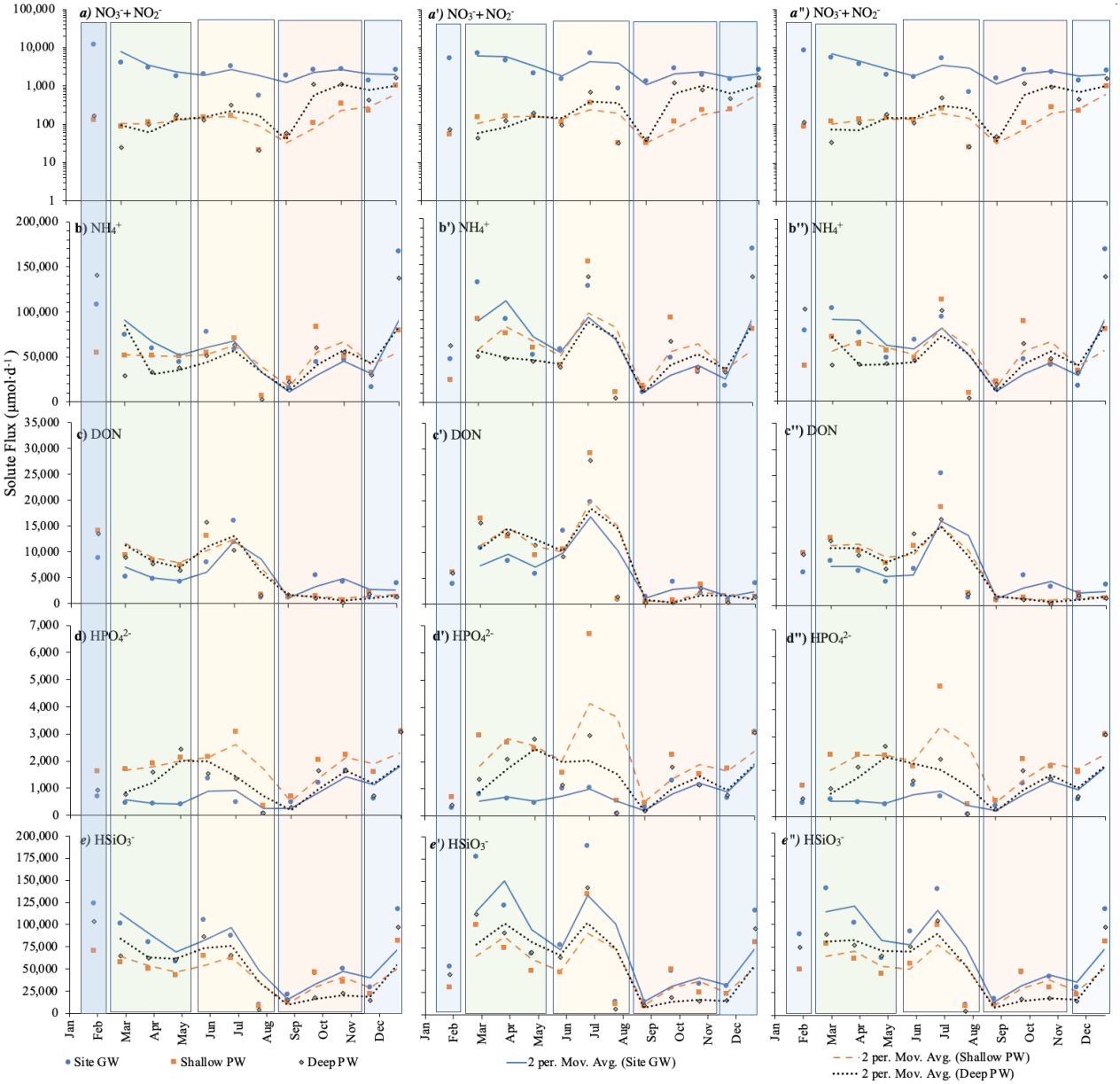

Figure 21. Nutrient fluxes per square meter of seepage face for a-e) LS, a'-e') RP and a"-e") average of both LS and RP. Solute fluxes were calculated using the site-specific SGD rate and the average solute concentration for both sites. Vertical colored panels represent seasons (blue – winter includes December, January, and February; green – spring includes March, April, and May; yellow – summer includes June, July, and August; and orange – fall, includes September, October, and November).

The highest NH_4^+ flux was measured at LS in February 2021 (167,311 µmol·d^{-1}; terrestrial) and at RP in July 2020 (152,959 µmol·d^{-1}; shallow porewater) while the lowest (2,584 µmol·d^{-1}; shallow porewater) transpired in August (Figure 21b') at LS. Overall, fluxes at RP

decreased throughout the monitoring period, although there were significant fluctuations. At LS, NH_4^+ fluxes showed a decreasing trend from February to August and increased again until January 2021 (Figure 21b).

Fluxes of DON were overall highest in the first half of 2020 and peaked for both sites in June (Figure 21c, c', c"). Starting with July DON fluxes decreased significantly regardless of the source (terrestrial or pore) with the terrestrial inputs slightly exceeding those from porewater in October and November. The highest DON flux was estimated at RP in June from both shallow and deep porewater endmembers (29,268 and 27,874 $\mu mol \cdot d^{-1}$, respectively). The lowest DON fluxes occurred at RP with deep porewater as the source 224 $\mu mol \cdot d^{-1}$ in September, although October and December match closely. Similarly, using the deeper porewater as the source LS DON fluxes were 252 $\mu mol \cdot d^{-1}$ in November. Other nutrient fluxes such as phosphate (HPO_4^{2-}) and silicate ($HSiO_3^-$) vary by site and month during the study period. For instance, HPO_4^{2-} ranges between 6,691 $\mu mol \cdot d^{-1}$ at RP (using the shallow porewater as the source) in July to 81 $\mu mol \cdot d^{-1}$ at LS in August (using both deep and groundwater sources) (Figure 21d, d'). Overall, fluxes derived using the shallow porewater as the source/end-member exceed the deeper and local groundwater sources, indicating that there is an additional source of HPO_4^{2-} from the sediment. Phosphorus is binding to metals such as iron and aluminum and often retained in agricultural soils after decades of excessive fertilizer use (legacy P) (Weissman and Tully, 2020). Further analyses of metal contents in porewater would help elucidate sources of phosphate, but given previous observations in Baffin Bay (Murgulet, 2018), it is expected that iron is present in amounts significant to impact phosphate mobility.

Fluxes of $HSiO_3^-$, are within similar ranges as NH_4^+, but interestingly follow a similar pattern as DON (Figure 21e and e'). $HSiO_3^-$ fluxes were highest in the first half of 2020 and

peaked for both sites in early spring and summer (Figure 21c, c'). Starting with July fluxes decreased significantly regardless of the source (terrestrial or pore) and started peaking again in October and again in January 2021. Terrestrial inputs (e.g., using groundwater as the source) slightly exceed those from porewater throughout the entire monitoring period. The highest $HSiO_3^-$ flux was estimated at RP in June from both shallow and deep porewater endmembers (189,997 and 177,542 $\mu mol \cdot d^{-1}$, respectively). The lowest fluxes (3,981 $\mu mol \cdot d^{-1}$) occurred at LS with deep porewater as the source in August, although September and December match closely. Similarly, using the deeper porewater as the source RP DON fluxes were 6,237 $\mu mol \cdot d^{-1}$ in August.

SUMMARY

Results of this study indicate that sewage or septic effluent is the dominant DON source to Baffin Bay whether near septic system/residential dominated area (RP site) or near underdeveloped, more agricultural dominated area (LS site). The high sewage/septic influence can be attributed to septic effluent percolation to groundwater and/or wastewater discharge, but high DON concentrations and enriched δ^{15}N-DON in the groundwater may indicate the former. The sewage/septic contribution at RP-S1 (46.5 ± 4.9%), RP-S2 (45.9 ± 5.3%), LS-S1 (45.9 ± 6.9%) and LS-S2 (46.5 ± 8.6%) site shows no significant variation among the two sites and with distance from the shoreline. The highest sewage/septic contribution at RP-S1, RP-S2 and LS-S1 is observed in fall, summer, and fall, respectively. The high pulse of groundwater DON (and NH_4^+) in summer to early fall may be attributed to these observed inputs. The highest sewage/septic contribution at LS-S2 occurred in winter, and given the distance from residential homes, sewage discharge from upstream wastewater treatment plants is likely. Observed DON

SGD fluxes are the lowest in winter 2020-2021, thus supporting the surface pathway for DON entering the system in this season.

Both surface water locations at LS exhibit the least sewage/septic contribution (37.6% and 37.4%, respectively) but highest fertilizer (18.2% and 18.2%, respectively), livestock waste (21.8% and 21.6%, respectively) and atmospheric deposition (22.5% and 22.8%, respectively) contribution in spring. This is potentially the result of higher precipitation (the highest amounts for the duration of the study occurred in May), which is followed by an increase in SGD rates, only slightly shy to the rates following Hurricane Hanna. The least sewage/septic contribution (40.4% and 41.3%, respectively), highest fertilizer (17.3% and 17.4%, respectively), livestock waste (20.7% and 20.7%, respectively) and atmospheric deposition (21.7% and 20.6%, respectively) contribution at RP-S1 and PR-S2 in winter and fall, respectively. This is like at LS and can be explained by of the higher SGD fluxes that seemed to be elevated by Hurricane Hanna event at the end of July and additional precipitation in September. This explains the high DON input of fertilizer, livestock waste, and atmospheric deposition in fall at RP-S2. In winter, when precipitation and riverine/surface runoff input are lower, DON SGD fluxes were among the lowest measured. However, from the existent DON pool, the relative contribution of fertilizer, livestock waste and atmospheric deposition were the highest. A decreased flux of nearshore SGD leads lo lower inputs of septic and in turn decreases the DON flux but increase the contribution of fertilizer, livestock waste and atmospheric deposition. This is expected to bring in more inputs of NOx and NH_4^+, as indicated by the SGD-derived fluxes of these solutes, which as oppose to DON, are increasing in fall and winter.

REFERENCES CITED

Alaniz, R.T., Goodwin, R.H. (1974) Recent sediments of a hypersaline estuarine bay: Gulf Coast Association of Geological Societies. Transactions 24, 308-313.

Aluwihare, L.I., Repeta, D.J., Pantoja, S., Johnson, C.G. (2005) Two Chemically Distinct Pools of Organic Nitrogen Accumulate in the Ocean. Science 308, 1007.

An, S., Gardner, W.S. (2002) Dissimilatory nitrate reduction to ammonium (DNRA) as a nitrogen link, versus denitrification as a sink in a shallow estuary (Laguna Madre/Baffin Bay, Texas). Marine ecology. Progress series (Halstenbek) 237, 41-50.

APHA, (1992) Standard methods for the examination of water and wastewater 18th edition. Am. Public Heal. Assoc., Washington, DC.

Ashworth, J.B., Hopkins, J., (1995) Major and minor aquifers of Texas, in: Board, T.W.D. (Ed.), p. 69.

Beck, A.J., Rapaglia, J.P., Cochran, J.K., Bokuniewicz, H.J. (2007) Radium mass-balance in Jamaica Bay, NY: Evidence for a substantial flux of submarine groundwater. Marine Chemistry 106, 419-441.

Beck, A.J., Rapaglia, J.P., Cochran, J.K., Bokuniewicz, H.J., Yang, S. (2008) Submarine groundwater discharge to Great South Bay, NY, estimated using Ra isotopes. Marine Chemistry 109, 279-291.

Behrens, E.W. (1963) Buried Pleistocene river valleys in Aransas and Baffin bays, Texas. Publications of the Institute of Marine Science, University of Texas 9, 7-18.

Behrens, E.W. (1966) Surface salinities for Baffin Bay and Laguna Madre, Texas, April 1964-March 1966. Publications of the Institute of Marine Science, University of Texas 11, 168-179.

Bighash, P., Murgulet, D. (2015) Application of factor analysis and electrical resistivity to understand groundwater contributions to coastal embayments in semi-arid and hypersaline coastal settings. Science of the Total Environment 532, 688-701.

Breier, J.A., Breier, C.F., Edmonds, H.N. (2010) Seasonal dynamics of dissolved Ra isotopes in the semi-arid bays of south Texas. Marine Chemistry 122, 39-50.

Breuer, J.P. (1957) An ecological survey of Baffin and Alazan Bays, Texas: Publ., Inst. Mar. Sci 4, 134-155.

Brock, D. (2001) Uncertainties in Individual Estuary N-Loading Assessments. Nitrogen Loading in Coastal Water Bodies: An Atmospheric Perspective, 171-185.

Bronk, D.A. (2002) Dynamics of DON. Biogeochem. Mar. dissolved Org. matter, 153–247.

Burnett, W.C., Dulaiova, H. (2003) Estimating the dynamics of groundwater input into the coastal zone via continuous radon-222 measurements. Journal of environmental radioactivity 69, 21-35.

Buskey, E.J., Liu, H., Collumb, C., Bersano, J.G.F. (2001) The Decline and Recovery of a Persistent Texas Brown Tide Algal Bloom in the Laguna Madre (Texas, USA). Estuaries 24, 337-346.

Campbell, J., (2018) Investigating the isotopic composition of reactive nitrogen in a south texas extuary (Baffin Bay). TAMU-CC.

Chaillou, G., Couturier, M., Tommi-Morin, G., Rao, A.M. (2014) Total alkalinity and dissolved inorganic carbon production in groundwaters discharging through a sandy beach. Procedia Earth and Planetary Science 10, 88-99.

Charette, M.A., Buesseler, K.O., Andrews, J.E. (2001) Utility of radium isotopes for evaluating the input and transport of groundwater-derived nitrogen to a Cape Cod estuary. Limnology and Oceanography 46, 465-470.

Choi, W.-J., Kwak, J.-H., Lim, S.-S., Park, H.-J., Chang, S.X., Lee, S.-M., Arshad, M.A., Yun, S.-I., Kim, H.-Y. (2017) Synthetic fertilizer and livestock manure differently affect δ15N in the agricultural landscape: A review. Agriculture, Ecosystems & Environment 237, 1-15.

Coastal Bay Bends and Estuary Program, C. (2015) Coastal Bay Bends and Estuary Program website.

Conley, D.J., Paerl, H.W., Howarth, R.W., Boesch, D.F., Seitzinger, S.P., Havens, K.E., Lancelot, C., Likens, G.E. (2009) Controlling Eutrophication: Nitrogen and Phosphorus. Science 323, 1014-1015.

Corbett, D.R., Burnett, W.C., Cable, P.H., Clark, S.B. (1998) A multiple approach to the determination of radon fluxes from sediments. Journal of Radioanalytical and Nuclear Chemistry 236, 247-252.

Cornell, S., Rendell, A., Jickells, T. (1995) Atmospheric inputs of dissolved organic nitrogen to the oceans. Nature 376, 243.

Curt, M.D., Aguado, P., Sánchez, G., Bigeriego, M., Fernández, J. (2004) Nitrogen Isotope Ratios of Synthetic and Organic Sources of Nitrate Water Contamination in Spain. Water, Air and Soil Pollution 151, 135-142.

Dalrymple, D.W., (1964) Recent Sedimentary Facies of Baffin Bay, Texas, Geology. Rice University, University Microfilms, Inc., Ann Arbor, Michigan.

Dimova, N., Burnett, W., Horwitz, E., Lane-Smith, D. (2007) Automated measurement of 224Ra and 226Ra in water. Applied radiation and isotopes 65, 428-434.

Doi, H., Kikuchi, E., Shikano, S., Takagi, S. (2010) Differences in nitrogen and carbon stable isotopes between planktonic and benthic microalgae. Limnology 11, 185-192.

Douglas, A.R., Murgulet, D., Peterson, R.N. (2020) Submarine groundwater discharge in an anthropogenically disturbed, semi-arid estuary. Journal of Hydrology 580, 124369.

Driese, S.G., Nordt, L.C., Lynn, W.C., Stiles, C.A., Mora, C.I., Wilding, L.P. (2005) Distinguishing climate in the soil record using chemical trends in a Vertisol climosequence from the Texas Coast Prairie, and application to interpreting Paleozoic paleosols in the Appalachian Basin, USA. Journal of Sedimentary Research 75, 339-349.

Dulaiova, H., Burnett, W.C. (2008) Evaluation of the flushing rates of Apalachicola Bay, Florida via natural geochemical tracers. Marine Chemistry 109, 395-408.

Durridge Company Inc., (2017) RAD7 Radon Detector User Manual, Billerica, MA, USA.

Felix, J.D., Campbell, J., (2019) Investigating Reactive Nitrogen Sources that Stimulate Algal Blooms in Baffin Bay, Coastal Bend Bays & Estuaries Program.

Felix, J.D., Qiu, Y., Cox, A., (2021) Quantifying Septic Effluent Nitrogen Loading and Processing in the Baffin Bay Watershed, Coastal Bend Bays & Estuaries Program.

Fetter, C.W. (2001) Applied Hydrogeology, Fourth Edition ed. Prentice-Hall, Inc., Upper Sadle River, New Jersey.

Fisk, H.N. (1959) Padre Island and the Laguna Madre flats, coastal south Texas. 2nd Coastal Geography Confer, 103-151.

Folk, R.L., Siedlecka, A. (1974) The “schizohaline” environment: its sedimentary and diagenetic fabrics as exemplified by Late Paleozoic rocks of Bear Island, Svalbard. Sedimentary Geology 11, 1-15.

Fowler, D., Coyle, M., Skiba, U., Sutton, M.A., Cape, J.N., Reis, S., Sheppard, L.J., Jenkins, A., Grizzetti, B., Galloway, J.N. (2013) The global nitrogen cycle in the twenty-first century. Phil. Trans. R. Soc. B 368, 20130164.

George, P.G., Mace, R., Petrossian, R., (2011) Aquifers of Texas: Texas Water Development Board Report 380, p. 182.

Giblin, A.E., Gaines, A.G. (1990) Nitrogen inputs to a marine embayment: the importance of groundwater. Biogeochemistry 10, 309-328.

Giblin, A.E., Weston, N.B., Banta, G.T., Tucker, J., Hopkinson, C.S. (2010) The Effects of Salinity on Nitrogen Losses from an Oligohaline Estuarine Sediment. Estuaries and Coasts 33, 1054-1068.

Gonneea, M.E., Morris, P.J., Dulaiova, H., Charette, M.A. (2008) New perspectives on radium behavior within a subterranean estuary. Marine Chemistry 109, 250-267.

Granger, J., Sigman, D.M. (2009) Removal of nitrite with sulfamic acid for nitrate N and O isotope analysis with the denitrifier method. Rapid Communications in Mass Spectrometry 23, 3753-3762.

Granger, J., Wankel, S.D. (2016) Isotopic overprinting of nitrification on denitrification as a ubiquitous and unifying feature of environmental nitrogen cycling. Proceedings of the National Academy of Sciences of the United States of America 113, E6391-E6400.

Hadas, O., Altabet, M.A., Agnihotri, R. (2009) Seasonally varying nitrogen isotope biogeochemistry of particulate organic matter in Lake Kinneret, Israel. Limnology and Oceanography 54, 75-85.

Harrison, R.B., Turner, N.S., Hoyle, J.A., Krejsl, J., Tone, D.D., Henry, C.L., Isaksen, P.J., Xue, D. (2000) Treatment of Septic Effluent for Fecal Coliform and Nitrogen in Coarse-textured Soils: Use of Soil-only and Sand Filter Systems. Water, Air and Soil Pollution 124, 205-215.

Holmes, R.M., Peterson, B.J., Deegan, L.A., Hughes, J.E., Fry, B. (2000) Nitrogen biogeochemistry in the oligohaline zone of a New England estuary. Ecology 81, 416-432.

Hu, C., Muller-Karger, F.E., Swarzenski, P.W. (2006) Hurricanes, submarine groundwater discharge, and Florida's red tides. Geophysical Research Letters 33.

Hvorslev, M.J. (1951) Time lag and soil permeability in ground-water observations.

Jolly, I.D., McEwan, K.L., Holland, K.L. (2008) A review of groundwater-surface water interactions in arid/semi-arid wetlands and the consequences of salinity for wetland ecology. Ecohydrology 1, 43-58.

Kendall, C., Elliott, E.M., Wankel, S.D. (2007) Tracing Anthropogenic Inputs of Nitrogen to Ecosystems. Stable Isotopes in Ecology and Environmental Science, 375-449.

Kim, G., Burnett, W., Dulaiova, H., Swarzenski, P., Moore, W. (2001) Measurement of Ra-224 and Ra-226 activities in natural waters using a radon-in-air monitor. Environmental science & technology 35, 4680-4683.

Knapp, A.N., Sigman, D.M., Lipschultz, F. (2005a) N isotopic composition of dissolved organic nitrogen and nitrate at the Bermuda Atlantic Time-series Study site. Global Biogeochemical Cycles 19.

Knapp, A.N., Sigman, D.M., Lipschultz, F. (2005b) N isotopic composition of dissolved organic nitrogen and nitrate at the Bermuda Atlantic Time‐series Study site. Global Biogeochemical Cycles 19.

Knapp, A.N., Sigman, D.M., Lipschultz, F., Kustka, A.B., Capone, D.G. (2011a) Interbasin isotopic correspondence between upper-ocean bulk DON and subsurface nitrate and its implications for marine nitrogen cycling. Global Biogeochemical Cycles 25.

Knapp, A.N., Sigman, D.M., Lipschultz, F., Kustka, A.B., Capone, D.G. (2011b) Interbasin isotopic correspondence between upper‐ocean bulk DON and subsurface nitrate and its implications for marine nitrogen cycling. Global Biogeochemical Cycles 25.

Knee, K.L., Garcia-Solsona, E., Garcia-Orellana, J., Boehm, A.B., Paytan, A. (2011) Using radium isotopes to characterize water ages and coastal mixing rates: A sensitivity analysis. Limnology and Oceanography: Methods 9, 380-395.

Krest, J.M., Moore, W.S., Gardner, L.R., Morris, J.T. (2000) Marsh nutrient export supplied by groundwater discharge: Evidence from radium measurements. Global Biogeochemical Cycles 14, 167-176.

Kroeger, K.D., Swarzenski, P.W., Greenwood, W.J., Reich, C. (2007) Submarine groundwater discharge to Tampa Bay: Nutrient fluxes and biogeochemistry of the coastal aquifer. Marine Chemistry 104, 85-97.

Lambert, M.J., Burnett, W.C. (2003) Submarine groundwater discharge estimates at a Florida coastal site based on continuous radon measurements. Biogeochemistry 66, 55-73.

Lee, J.-M., Kim, G. (2006) A simple and rapid method for analyzing radon in coastal and ground waters using a radon-in-air monitor. Journal of environmental radioactivity 89, 219-228.

Lee, K.-S., Lee, D.-S., Lim, S.-S., Kwak, J.-H., Jeon, B.-J., Lee, S.-I., Lee, S.-M., Choi, W.-J. (2012) Nitrogen isotope ratios of dissolved organic nitrogen in wet precipitation in a metropolis surrounded by agricultural areas in southern Korea. Agriculture, Ecosystems & Environment 159, 161-169.

Lohse, E.A., (1955) Dynamic geology of the modern coastal region, northwest Gulf of Mexico, in: Hough, J.L. (Ed.), Finding Ancient Shorelines: A Symposium with Discussions. Society of Economic Paleontologists and Mineralogists Special Publication, pp. 99-104.

Lopez, C.V., Murgulet, D., Santos, I.R. (2020) Radioactive and stable isotope measurements reveal saline submarine groundwater discharge in a semiarid estuary. Journal of Hydrology 590, 125395.

Lusk, M.G., Toor, G.S., Yang, Y.-Y., Mechtensimer, S., De, M., Obreza, T.A. (2017) A review of the fate and transport of nitrogen, phosphorus, pathogens, and trace organic chemicals in septic systems. Critical Reviews in Environmental Science and Technology 47, 455-541.

Matson, E.A. (1993) Nutrient flux through soils and aquifers to the coastal zone of Guam (Mariana Islands). Limnology and Oceanography 38, 361-371.

McGonigle, T.P., Beauchamp, E.G., Evans, L.J., Wells, C.J. (2012) Mineralization and Crop Uptake of Nitrogen from Textile Manufacturing Wastewater Sludge Cake. Applied and Environmental Soil Science 2012, 273456.

Militello, A., (1998) Hydrodynamics of wind-dominated, shallow embayments. Florida Institute of Technology, Melbourne, FL, p. 232.

Möbius, J. (2013) Isotope fractionation during nitrogen remineralization (ammonification): Implications for nitrogen isotope biogeochemistry. Geochimica et Cosmochimica Acta 105, 422-432.

Moore, J.W., Semmens, B.X. (2008) Incorporating uncertainty and prior information into stable isotope mixing models. Ecology Letters 11, 470-480.

Moore, W., (1996a) Large groundwater inputs to coastal waters revealed by 226Ra enrichments.--p. 612-614. En: Nature (London)(United Kingdom).--Vol. 380, no. 6575 (1996).

Moore, W.S. (1996b) Large groundwater inputs to coastal waters revealed by Ra-226 enrichments. Nature 380, 612-614.

Moore, W.S. (2000a) Ages of continental shelf waters determined from 223Ra and 224Ra. Journal of Geophysical Research: Oceans 105, 22117-22122.

Moore, W.S. (2000b) Determining coastal mixing rates using radium isotopes. Continental Shelf Research 20, 1993-2007.

Moore, W.S. (2006) Radium isotopes as tracers of submarine groundwater discharge in Sicily. Continental Shelf Research 26, 852-861.

Moore, W.S. (2010) The effect of submarine groundwater discharge on the ocean. Annual review of marine science 2, 59-88.

Murgulet, D. (2018) Impacts of Temporal and Spatial Variation of Submarine Groundwater Discharge on Nutrient
Fluxes to Texas Coastal Embayments, Phase III (Baffin Bay). Texas General Land Office.

Nikolenko, O., Jurado, A., Borges, A.V., Knöller, K., Brouyère, S. (2018) Isotopic composition of nitrogen species in groundwater under agricultural areas: A review. Science of the Total Environment 621, 1415-1432.

NOAA/CO-OPS, (2021) Baffin Bay, TX - Station ID: 8776604, in: NOAA (Ed.). NOAA & CO-OPS.

NREL, (2007) The 1991–2005 National Solar Radiation Database, in: Laboratory, N.R.E. (Ed.).

Paerl, H.W. (1997) Coastal eutrophication and harmful algal blooms: Importance of atmospheric deposition and groundwater as “new” nitrogen and other nutrient sources. Limnology and Oceanography 42, 1154-1165.

Parnell, A.C., Inger, R., Bearhop, S., Jackson, A.L. (2010) Source Partitioning Using Stable Isotopes: Coping with Too Much Variation. PloS one 5, e9672.

Parnell, A.C., Phillips, D.L., Bearhop, S., Semmens, B.X., Ward, E.J., Moore, J.W., Jackson, A.L., Grey, J., Kelly, D.J., Inger, R. (2013) Bayesian stable isotope mixing models. Environmetrics 24, 387-399.

Peterson, R.N., Burnett, W.C., Taniguchi, M., Chen, J., Santos, I.R., Ishitobi, T. (2008) Radon and radium isotope assessment of submarine groundwater discharge in the Yellow River delta, China. Journal of Geophysical Research 113.

Price, W.A. (1936) Reynosa problem of South Texas, and origin of caliche.

Prokopenko, M., Sigman, D., Berelson, W., Hammond, D., Barnett, B., Chong, L., Townsend-Small, A. (2011) Denitrification in anoxic sediments supported by biological nitrate transport. Geochimica et Cosmochimica Acta 75, 7180-7199.

Qiu, Y., Felix, J.D., Cox, A., Murgulet, D., (Unpublished work) Using Stable Isotopes to Determine Sources and Processing of Inorganic and Organic Nitrogen in a Septic System Dominated versus Undeveloped Estuary Coastline.

RCRA SOP, (2009) Protocol for Groundwater/Surface Water Interface Sampling Using a Pore Water Sampler, in: Beneski, B., Bonenfant, E. (Eds.), Standard Operating Procedure Change Record. Department of Environmental Protection Bureau of Remediation and Waste Management RCRA Program.

Rebich, R.A., Houston, N.A., Mize, S.V., Pearson, D.K., Ging, P.B., Evan Hornig, C. (2011) Sources and Delivery of Nutrients to the Northwestern Gulf of Mexico from Streams in the South-Central United States. JAWRA Journal of the American Water Resources Association 47, 1061-1086.

Robinson, C.E., Xin, P., Santos, I.R., Charette, M.A., Li, L., Barry, D.A. (2018) Groundwater dynamics in subterranean estuaries of coastal unconfined aquifers: Controls on submarine groundwater discharge and chemical inputs to the ocean. Advances in Water Resources 115, 315-331.

Rodellas, V., Stieglitz, T.C., Tamborski, J.J., van Beek, P., Andrisoa, A., Cook, P.G. (2021) Conceptual uncertainties in groundwater and porewater fluxes estimated by radon and radium mass balances. Limnology and Oceanography.

Rusnak, G.A., (1960) Sediments of Laguna Madre, Texas, in: Shepard, F.P., Phleger, F.B., Van Andal, T.H. (Eds.), Recent Sediments, Northwest Gulf of Mexico. American Association of Petroleum Geologists, Tulsa OK, pp. 153-196.

Russell, K.M., Galloway, J.N., Macko, S.A., Moody, J.L., Scudlark, J.R. (1998) Sources of nitrogen in wet deposition to the Chesapeake Bay region. Atmospheric Environment 32, 2453-2465.

Sadat-Noori, M., Santos, I.R., Tait, D.R., Maher, D.T. (2016) Fresh meteoric versus recirculated saline groundwater nutrient inputs into a subtropical estuary. Science of the Total Environment 566, 1440-1453.

Santos, I.R., Cook, P.L., Rogers, L., Weys, J.d., Eyre, B.D. (2012) The “salt wedge pump”: Convection-driven pore-water exchange as a source of dissolved organic and inorganic carbon and nitrogen to an estuary. Limnology and Oceanography 57, 1415-1426.

Scavia, D., Bricker, S.B., (2006) Coastal eutrophication assessment in the United States, Nitrogen Cycling in the Americas: Natural and Anthropogenic Influences and Controls. Springer, pp. 187-208.

Schlarbaum, T., Daehnke, K., Emeis, K. (2010) Turnover of combined dissolved organic nitrogen and ammonium in the Elbe estuary/NW Europe: results of nitrogen isotope investigations. Marine Chemistry 119, 91-107.

Schulz, H.D., Dahmke, A., Schinzel, U., Wallmann, K., Zabel, M. (1994) Early diagenetic processes, fluxes, and reaction rates in sediments of the South Atlantic. Geochimica et Cosmochimica Acta 58, 2041-2060.

Sigman, D.M., Casciotti, K.L., Andreani, M., Barford, C., Galanter, M., Böhlke, J.K. (2001) A Bacterial Method for the Nitrogen Isotopic Analysis of Nitrate in Seawater and Freshwater. Analytical Chemistry 73, 4145-4153.

Sigman, D.M., Karsh, K., Casciotti, K. (2009) Ocean process tracers: nitrogen isotopes in the ocean.

Simms, A.R., Aryal, N., Miller, L., Yokoyama, Y. (2010) The incised valley of Baffin Bay, Texas: a tale of two climates. Sedimentology 57, 642-669.

Smith, C.G., Robbins, L.L., (2012) Surface-Water Radon-222 Distribution along the Western-Central Florida Shelf. U.S. Geological Survey, p. 26.

Sorooshian, S., Hsu, K., Braithwaite, D., Ashouri, H., Program, N.C., (2014) NOAA Climate Data Record (CDR) of Precipitation Estimation from Remotely Sensed Information using Artificial Neural Networks (PERSIANN-CDR), in: Information, N.N.C.f.E. (Ed.), Precipitation, Version 1 Revision 1 ed.

Spalt, N., Murgulet, D., Abdulla, H. (2019) Spatial variation and availability of nutrients at an oyster reef in relation to submarine groundwater discharge. Science of the Total Environment, 136283.

Spalt, N., Murgulet, D., Hu, X. (2018) Relating estuarine geology to groundwater discharge at an oyster reef in Copano Bay, TX. Journal of Hydrology 564, 785-801.

Sun, Y., Torgersen, T. (1998) The effects of water content and Mn-fiber surface conditions on 224Ra measurement by 220Rn emanation. Marine Chemistry 62, 299-306.

Swarzenski, P.W., Reich, C., Kroeger, K.D., Baskaran, M. (2007) Ra and Rn isotopes as natural tracers of submarine groundwater discharge in Tampa Bay, Florida. Marine Chemistry 104, 69-84.

Tait, D.R., Maher, D.T., Sanders, C.J., Santos, I.R. (2017) Radium-derived porewater exchange and dissolved N and P fluxes in mangroves. Geochimica et Cosmochimica Acta 200, 295-309.

TCEQ, (2012) Surface Water Quality Monitoring Procedures, Volume 1: Physical and Chemical Monitoring Methods, Austin, TX.

TCOON, (2016) Historical Standard Meteorological Data - Station BABT2 - 8776604 - Baffin Bay, TX, in: Network, T.C.O.O. (Ed.). National Oceanic and Atmospheric Administration, National Data Buoy Center.

Tsunogai, U., Kido, T., Hirota, A., Ohkubo, S.B., Komatsu, D.D., Nakagawa, F. (2008a) Sensitive determinations of stable nitrogen isotopic composition of organic nitrogen through chemical conversion into N2O. Rapid Communications in Mass Spectrometry: An International Journal Devoted to the Rapid Dissemination of Up ‐ to ‐ the ‐ Minute Research in Mass Spectrometry 22, 345-354.

Tsunogai, U., Kido, T., Hirota, A., Ohkubo, S.B., Komatsu, D.D., Nakagawa, F. (2008b) Sensitive determinations of stable nitrogen isotopic composition of organic nitrogen through chemical conversion into N2O. Rapid Communications in Mass Spectrometry 22, 345-354.

TWDB, (2019a) Hydrology for the Laguna Madre Estuary Watershed, in: Studies, C.f.W.S. (Ed.).

TWDB, (2019b) Hydrology for the Nueces Bay Estuary Watershed, in: Studies, C.f.W.S. (Ed.).

TWDB, (2019c) Hydrology of the Lamar Peninsula, in: Studies, C.f.W.S. (Ed.).

Uddameri, V., Singaraju, S., Hernandez, E.A. (2013) Temporal variability of freshwater and pore water recirculation components of submarine groundwater discharges at Baffin Bay, Texas. Environmental Earth Sciences 71, 2517-2533.

USGS, (2017a) USGS 08211900 San Fernando Ck at Alice, TX, in: Inquiries, U.T.W.S.C.W.-D. (Ed.). National Water Information System: Web Interface.

USGS, (2017b) USGS 08212400 Los Olmos Ck nr Falfurrias, TX, in: Center, U.T.W.S. (Ed.). National Water Information System: Web Interface.

USGS, (2019a) USGS 08211520 Oso Ck at Corpus Christi, TX, in: Inquiries, U.T.W.S.C.W.-D. (Ed.). National Water Information System: Web Interface.

USGS, (2019b) USGS 08212400 Los Olmos Ck nr Falfurrias, TX, in: Center, U.T.W.S. (Ed.). National Water Information System: Web Interface.

USGS, (2021a) USGS 08211900 San Fernando Ck at Alice, TX, in: USGS (Ed.), National Water Information System: Web Interface.

USGS, (2021b) USGS 08212400 Los Olmos Ck nr Falfurrias, TX. National Water Information System: Web Interface.

USGS, (2021c) USGS 08212820 Petronila Ck at FM 665 nr Driscoll, TX, in: USGS (Ed.). USGS, National Water Information System: Web Interface.

Vähätalo, A.V., Järvinen, M. (2007) Photochemically produced bioavailable nitrogen from biologically recalcitrant dissolved organic matter stimulates production of a nitrogen-limited microbial food web in the Baltic Sea. Limnology and Oceanography 52, 132-143.

Ward, G.H., Armstrong, N.E. (1997) Current Status and Historical Trends of Ambient Water, Sediment, Fish and Shellfish Tissue Quality in the Corpus Christi Bay National Estuary Program Study Area: Summary Report. Natural Resources Center, TAMU-CC.

Waterstone, Parsons, (2003) Groundwater availability of the central Gulf Coast aquifer--Numerical simulations to 2050, Central Gulf Coast, Texas.

Weissman, D.S., Tully, K.L. (2020) Saltwater intrusion affects nutrient concentrations in soil porewater and surface waters of coastal habitats. Ecosphere 11, e03041.

Wells, N.S., Eyre, B.D. (2019) δ15N patterns in three subtropical estuaries show switch from nitrogen “reactors” to “pipes” with increasing degradation. Limnology and Oceanography 64, 860-876.

Wetz, M.S., (2015) Baffin Bay Volunteer Water Quality Monitoring Study: Synthesis of May 2013-July 2015 Data. Coastal Bend Bays & Estuaries Program, pp. 1-28.

Wetz, M.S., Cira, E.K., Sterba-Boatwright, B., Montagna, P.A., Palmer, T.A., Hayes, K.C. (2017) Exceptionally high organic nitrogen concentrations in a semi-arid South Texas estuary susceptible to brown tide blooms. Estuarine, Coastal and Shelf Science 188, 27-37.

WSDE, (2017) Nitrogen from Atmospheric Deposition. Washington State Department of Ecology.

Young, S. (2016) Desired future condition explanatory report for Groundwater Management Area 15. Texas Water Development Board Report.